ILINA MUTAPČIĆ, BSc

CONFORMATIONAL ANALYSIS OF BIS(L-HISTIDINATO)COPPER(II) VIA QUANTUM CHEMICAL DFT CALCULATIONS

MASTER THESIS

FOR THE ACADEMIC DEGREE OF

DIPLOM-INGENIEURIN

IN THE MASTER'S DEGREE PROGRAMME TECHNICAL CHEMISTRY

SUBMITTED TO

GRAZ UNIVERSITY OF TECHNOLOGY

SUPERVISOR:

DR. RAMEK MICHAEL, AO.UNIV.-PROF.

INSTITUTE OF PHYSICAL AND THEORETICAL CHEMISTRY

GRAZ, MARCH 2019

EIDESSTATTLICHE ERKLÄRUNG

Ich erkläre an Eides statt, dass ich die vorliegende Arbeit selbstständig verfasst, andere als die angegebenen Quellen/Hilfsmittel nicht benutzt, und die den benutzten Quellen wörtlich und inhaltlich entnommenen Stellen als solche kenntlich gemacht habe. Das in TUGRAZonline hochgeladene Textdokument ist mit der vorliegenden Masterarbeit identisch.

18. APRIL 2019

Datum

Unterschrift

CONTENT

ABSTRACT

This study examines the structural characteristics of the physiological complex bis(L-histidinato)copper(II) [Cu(L-His)$_2$] in gas phase when the proton is shifted from one nitrogen (N$_\tau$) to the other (N$_\pi$) within the imidazole ring in at least one L-His side chain. The four possible donor atoms in this complex are the amino nitrogen N$_{am}$, the carboxylate oxygen O and the two imidazole nitrogen atoms, N$_\tau$ and N$_\pi$. It is studied, how hydrogen bonding and apical coordination affect the stability of this Cu(L-His)$_2$ complex in the following coordination modes: glycine-like mode, in which copper binds via N$_{am}$ and O (G mode), histamine-like mode via N$_{am}$ and N$_\pi$ (H mode) and imidazole-propionic acid-like mode via N$_\pi$ and O (I mode). To distinguish between the L-His residue with the proton on N$_\tau$ and the L-His residue with protonated N$_\pi$, the letter p for "proton shifted" was added to the respective coordination mode for the latter case. For the conformational analysis of these conformers, the density functional theory (DFT) method with the B3LYP functional was used. In the I and Ip mode a new coordination type was established during this analysis, in which both oxygen atoms from the same carboxylate group bind to copper(II) and form a four-membered chelate ring. This is indicated by *2* instead of *cis* and *trans* in the conformer names. A total of 466 equilibrium structures are obtained: 219 in *trans* configuration, 210 in *cis* configuration and 37 in *2* configuration.

In general, the order of the coordination modes in terms of stability is: tGGp < tGpGp < tIGp < cHGp < cGGp < cGpGp < cIGp < 2IGp < 2IpGp < tHGp with the most stable *trans* configuration in the GGp mode and the least stable *trans* configuration in the HGp mode. *Inter-* and *intra-*residual hydrogen bonds have a significant stabilization effect on the complex, as well as apical bonding. Most hydrogen bonds are formed within one L-His residue, whereas *inter* ones occur less often. Concerning apical bonds in the equilibrium structures, only two donor atoms formed axial bonds to copper(II): N$_\pi$ and N$_{am}$. Neither N$_\tau$ binds to copper, despite the electron lone pair due to the proton shift to N$_\pi$, nor any of the carboxyl oxygen atoms.

The most stable conformer is a *trans* GGp with an electronic energy of −1292.77081 a.u. that forms an apical bond Cu–N$_\pi$ in the G residue and an *intra-*residual hydrogen bond N$_\pi$–H···O in the Gp residue. The previously known most stable conformer (with N$_\tau$ protonated in both L-His side chains) is 8.43 kJ mol^{-1} less stable, which means that a new global minimum structure for this complex was found in this study.

ACKNOWLEDGEMENT

INTRODUCTION

Half a century ago, a new disease was discovered that manifested itself in babies by peculiar hair growth and an otherwise complex clinical presentation [1]. It was first named Menkes syndrome after its discoverer, but soon the name changed to Menkes disease. Neither cause nor any kind of treatment were known at that time. This changed about 10 years later, when David M. Danks realized the similarity of the symptoms with those observed in copper-deficient sheep [2] [3] [4]. This initiated an experimental treatment with copper(II) salts [5] [6] [7]; the gene responsible for Menkes disease was located in 1993 [8] [9] [10]. Since 2012, copper(II) diaminoacid complexes are studied in an ongoing project by J. Sabolović and co-workers: Cu(L-His)$_2$ [11] [12] [13], Cu(L-His)(L-Thr) [14], Cu(L-Thr)$_2$ and Cu(L-*allo*-Thr)$_2$ [15], Cu(L-Cys)(L-Asn) [16], Cu(L-Asn)$_2$ [17] and Cu(L-His)(L-Asn) [18]. In this project, the structure of the amino acids (aa) is assumed to be deprotonated at the carboxyl group in order to get the intended negative charge; together with Cu^{2+} this will yield electroneutral Cu(aa)$_2$ salts. In the part of Cu(L-His)$_2$, the side chain of L-histidine was assumed to be always protonated at N_τ (Figure 1). In the work on Cu(L-His)(L-Thr) [14] it became evident that structures, in which the proton is shifted from N_τ to N_π, also yield comparative energies. This finding triggered the present work, the topic of which is a re-investigation of the Cu(L-His)$_2$ potential energy surface with such a proton shift in either one or both L-histidine residues.
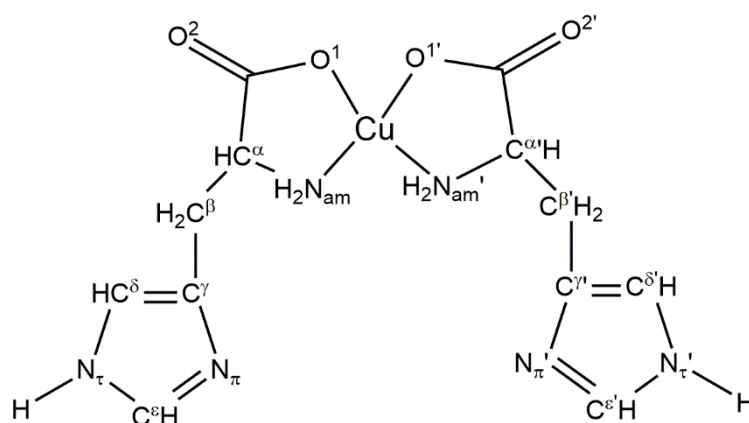
Figure 1: Definition of the atom labelling, using the example of one possible chelation mode of Cu(L-His)$_2$ protonated at N_τ on both side chains.

METHODS

2.1. CONSTRUCTION OF INITIAL CONFORMATIONS

The L-histidine residue contains an imidazole group with two nitrogen atoms, N_π and N_τ, only one of which is protonated in the biologically significant pH range of 6–7. While in copper proteins L-His usually binds to the copper ion only via an unprotonated imidazole N atom [19], it can coordinate in low-molecular-weight $Cu(aa)_2$ complexes bidentately or tridentately via three possible donor atoms, which are indicated in Figure 2: the carboxylate oxygen (O^1), the unprotonated imidazole nitrogen (either N_π or N_τ) and the amino nitrogen (N_{am}) [20] [21].
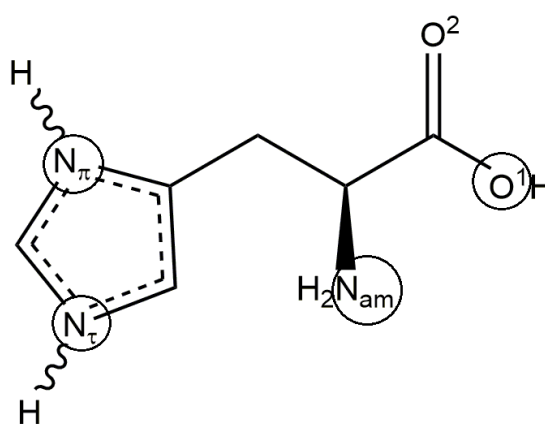
Figure 2: L-Histidine, a potentially tridentate ligand.

Protonation of N_τ leads to three possible chelation modes: the glycine-like mode (via N_{am} and O^1), the histamine-like mode (via N_{am} and N_π) and the imidazole-propionic acid-like mode (via N_π and O^1). By shifting the proton from N_τ to N_π, two more chelation modes are possible: the proton-shifted glycine-like mode (via N_{am} and O^1) and the proton-shifted imidazole-propionic acid-like mode (N_τ and O^1). In this work, they are termed as G, H, I, Gp and Ip modes, respectively. These possible chelation modes are depicted in Figure 3.

G mode

H mode

I mode

Gp mode

Ip mode
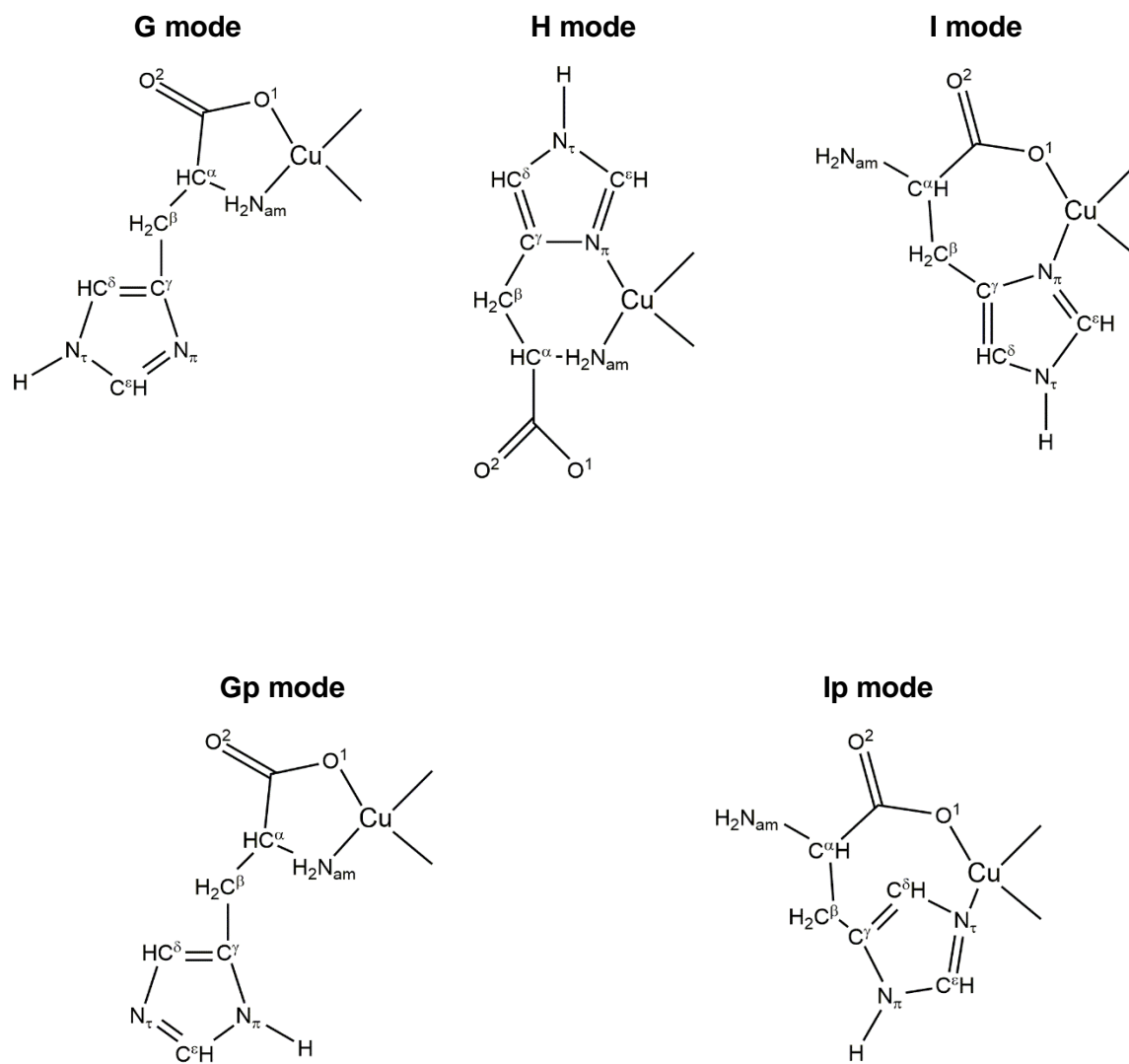
Figure 3: The five chelation modes of L-His to Cu(II) studied in this work.

The construction of initial structures for the different L-His conformers was based on the conformational analysis of Cu(L-His)$_2$ described in a previous work [12] but with a proton shift from N$_\tau$ to N$_\pi$ in at least one L-His residue. This leads to 5 combined coordination modes: GGp, GpGp, HGp, IGp and IpGp, which are illustrated in Figure 4. In each of these, the two N$_{am}$ or O^1 atoms can be either in a *trans* or *cis* position in the equatorial plane, denoted as "t" and "c" in the conformer names. During the optimization a third arrangement around copper(II) was found: two binding carboxylate oxygen atoms, O^1 and O^2, forming a four-membered chelate ring with copper(II). This case is indicated by "2" instead of "c" and "t" at the beginning of the symbol. A number of initial structures in the IpG coordination mode was constructed too, but optimized to complexes with less than four coordinating atoms to Cu(II) and were therefore not further analyzed.

GGp mode

GpGp mode

HGp mode
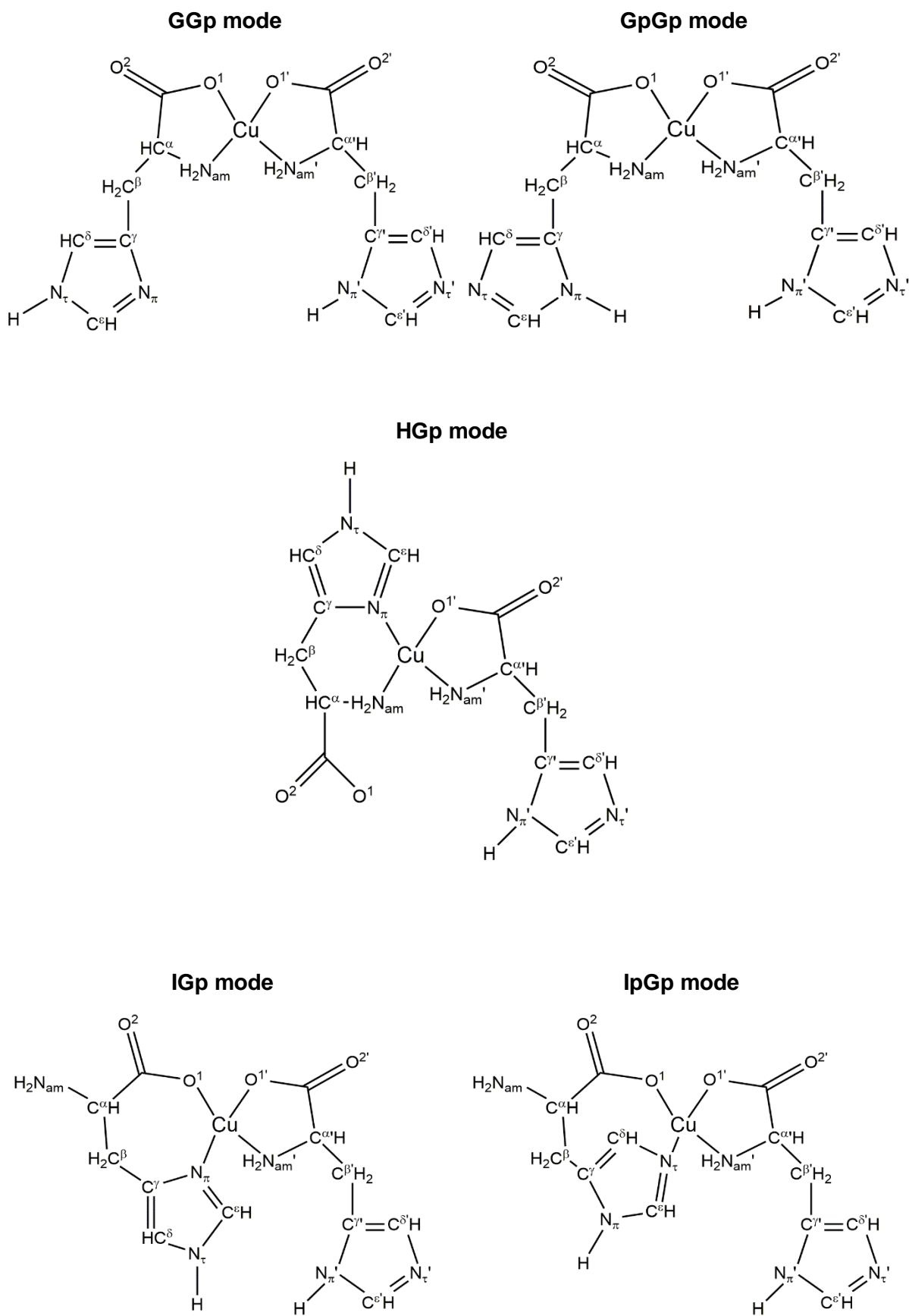
IGp mode

IpGp mode

Figure 4: Cis coordination modes of Cu(L-His)₂ when the proton is shifted from Nτ to Nπ either in one or both L-His residues.

2.1.1. GLYCINE-LIKE MODES (G AND GP MODE)

In the G and Gp mode, the five-membered chelate ring can have two conformations, leading to structures with the C^β atom in an axial or an equatorial position. These are denoted as "a" and "e" in the conformer names (Figure 5). The axial and equatorial position were constructed by setting the torsion angles $Cu–N_{am}–C^\alpha–C$ and $N_{am}–C^\alpha–C–O^1$ to 28 and –21° for the axial and –32° and 22° for the equatorial position, respectively.

We assumed that the torsion angle $N_{am}–C^\alpha–C^\beta–C^\gamma$ can adopt the characteristic values –60°, 60° and 180°. The other L-His residue angle, $C^\alpha–C^\beta–C^\gamma–C^\delta$, seemed less predictable, hence initial values of ±60°, ±120° and 180° were used in the G mode. Based on the outcome, for the Gp mode more specific values were selected, which are listed in Table 1.

Table 1: Initial torsion angles for the five-membered chelate ring orientation in the Gp mode.

$N_{am}–C^\alpha–C^\beta–C^\gamma$		$C^\alpha–C^\beta–C^\gamma–C^\delta$
60°	–106°	43°
–60°	90°	–30°
180°	120°	–68°

To construct the *cis* and *trans* geometries, the valence angles $N_{am}–Cu–N_{am}'$ or $N_{am}–Cu–O^{1'}$ were set to 90° for *cis* and *trans*, respectively. Combining these assumptions led to 1800 GGp and 156 GpGp initial structures.

2.1.2. HISTAMINE-LIKE MODE (H MODE)

In the H mode, the six-membered chelate ring can have two conformations, both with a reference plane defined by Cu(II), N_π and N_{am}. The C^β atom can be positioned above the plane, while the C^α and carboxyl group atoms are placed below the plane and vice versa. The carboxylate group is then axial or equatorial relative to the plane around copper(II), hence we named these structures "a" and "e". Initial structures were generated with a value of –30° and 30° for the torsion angle $Cu–N_{am}–C^\alpha–C^\beta$ for axial and equatorial, respectively. For the second relevant torsion angle for this mode, $N_{am}–C^\alpha–C^\beta–C^\gamma$, we used initial values of 0° and 90°, labelled "1" and "2", respectively. *Cis* and *trans* conformers were constructed in the same way as in the G mode, by setting the valence angle $N_{am}–Cu–N_{am}'$ to 90° for *cis*, and $N_{am}–Cu–O^{1'}$ to 90° for *trans* conformers. Combining this H chelation mode of one L-His residue with the proton shifted G mode of the other L-His residue led to a total of 240 HGp initial structures.

2.1.3. IMIDAZOLE-PROPIONIC ACID-LIKE MODES (I AND IP MODE)

The seven-membered chelate ring in the I mode can also adopt two conformations, with the N_{am} atom in an axial position relative to the other chelate-ring atoms (resembling a boat conformation) or in an equatorial position (resembling a chair conformation). 6 initial conformations of the seven-membered ring were used that we distinguished by the combination of $Cu–N_\pi–C^\gamma–C^\beta$ (~15°) and torsion angle triplets for $N_\pi–C^\gamma–C^\beta–C^\alpha$, $C^\gamma–C^\beta–C^\alpha–C$ and $C^\beta–C^\alpha–C–O^1$. The values of these triplets were set to: 70°, –50°, –50° *(b1);* –60°, 60°, –90° *(b2);* –70°, 50°, 50° *(b3);* 60°, –66°, 94° *(b4);* 30°, 50°, –90° *(b5)* and –30°, –50°, 90° *(b6).* *Cis* and *trans* conformers were constructed by setting the valence angle $O^1–Cu–O^{1'}$ to 90° for *cis*, and $N_{am}–Cu–O^{1'}$ to 90° for *trans* conformers. Combining all these I mode combinations with the Gp mode led to 360 IGp initial structures.

When the proton is shifted from N_τ to N_π, an eight-membered chelate ring can be formed, which corresponds to the Ip mode. *Cis* and *trans* conformers were created the same way as in the other modes. Four initial conformations of the eight-membered chelate ring were used that are defined in Table 2, resulting in a total of 240 IpGp structures.

Table 2: Initial conformations of the eight-membered chelate ring in the Ip mode.

	1	2	3	4
$Cu–N_\tau–C^\delta–C^\gamma$	104.0°	88.0°	–102.0°	–102.0°
$N_\tau–C^\delta–C^\gamma–C^\beta$	–150.0°	–147.0°	153.0°	153.0°
$C^\delta–C^\gamma–C^\beta–C^\alpha$	90.0°	105.0°	–83.0°	–83.0°
$C^\gamma–C^\beta–C^\alpha–C$	–49.0°	–38.6°	–10.0°	40.0°
$C^\beta–C^\alpha–C–O^1$	92.0°	152.5°	92.0°	92.0°
$N_\tau–C^\delta–C^\gamma–N_\pi$	5.0°	5.0°	5.0°	5.0°
$C^\delta–C^\gamma–N_\pi–C^\epsilon$	–4.0°	–4.0°	–4.0°	–4.0°

2.2. QUANTUM CHEMICAL CALCULATIONS

The neutral molecule $Cu(L\text{-His})_2$ has a spin multiplicity of 2. For compatibility with already existing data, the calculations were carried out in the same way as in previous work [12] by using the unrestricted DFT method with the B3LYP hybrid density functional [22] [23] [24] [25] and the LanL2DZ double-ζ basis set [26], extended by a set of polarization [27] and diffuse

functions [28] on N, O, and C. The nonrelativistic effective-core potentials (ECPs) of Hay and Wadt (LanL2DZ) were used to describe the shielding effects of electrons in the copper inner shells [29] [30] [31]. To verify whether the optimized geometries are local minima, frequency calculations were performed to ensure the absence of imaginary frequencies. For all the quantum chemical calculations the *Gaussian09* program package was used [32].

RESULTS AND DISCUSSION

3.1. GEOMETRY OPTIMIZATIONS

From a total of 2796 initial structures, 466 equilibrium structures were obtained. The most stable *cis, trans* and *2* conformations of each coordination mode are illustrated in Figure 5. The conformers with the lowest electronic energy are tGGp_a19_e12 for the *trans* conformation, and cHGp_a2_a17 for the *cis* conformation (the conformer nomenclature is given below). The *trans* conformer is the most stable one with an electronic energy of −1292.770814 a.u. (Figure 5).

GGp mode

tGGp_a19_e12   cGGp_a18_a12
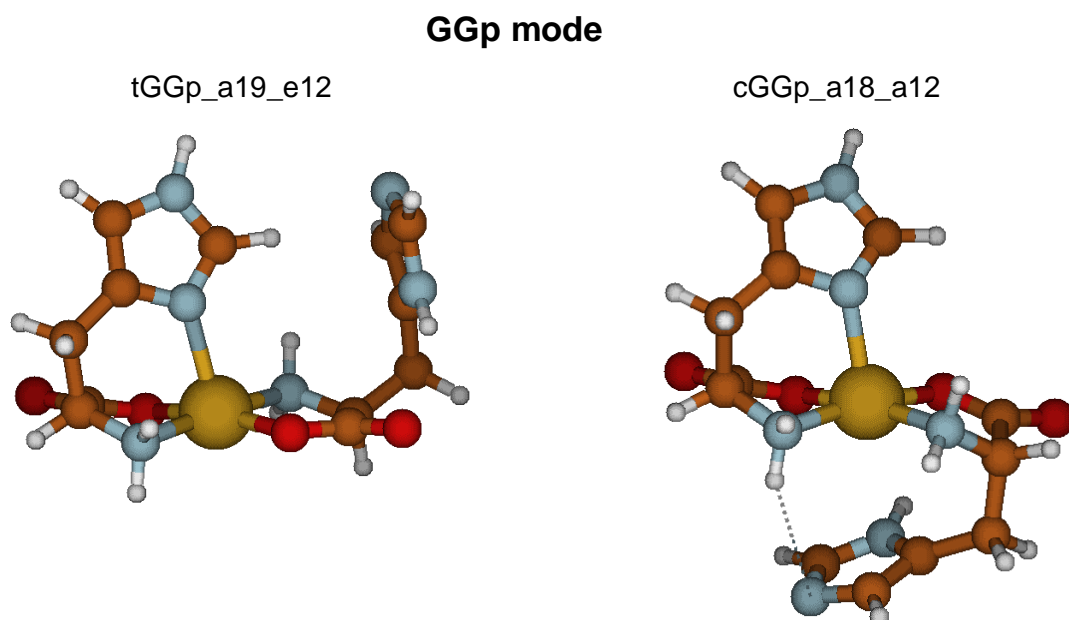
Figure 5: Most stable existing cis, trans and 2 equilibrium conformations of each coordination mode.

GpGp
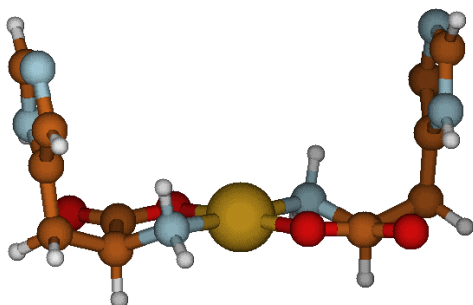
tGpGp_e12_e12_A   cGpGp_a12_a12
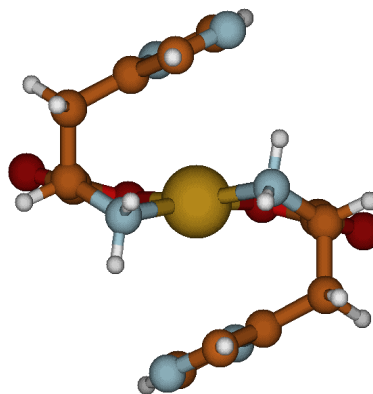
HGp
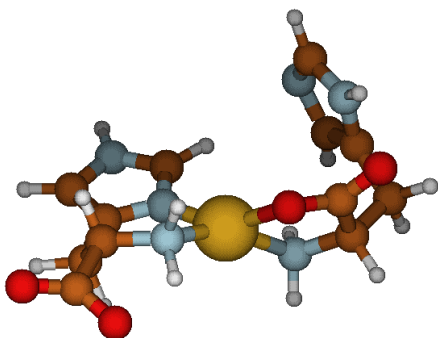
tHGp_e1_e12   cHGp_a2_a17
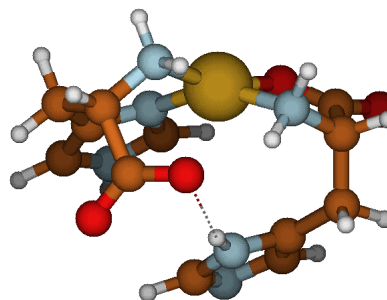
IGp
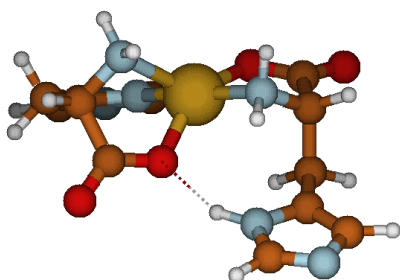
tIGp_sb6_a22   cIGp_sb6_e12
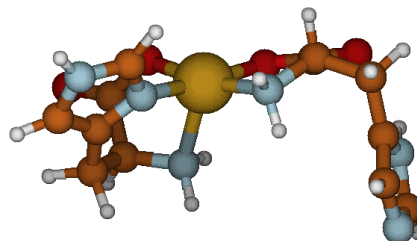
Figure 5 (continued).

2IGp_ub7_e12

IpGp
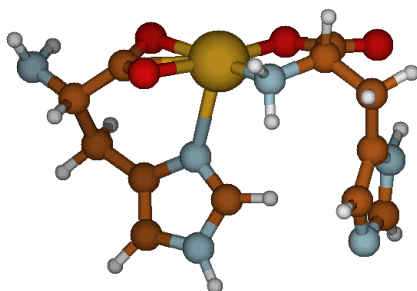
2IpGp_m2_a24
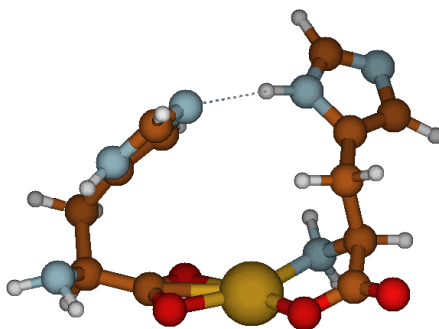
Figure 5 (continued).

3.1.1. GLYCINE-LIKE MODES (G AND GP MODE)

In the case of the *trans* position, the valence angle N_{am}–Cu–N_{am}' is above 140° and in the *cis* position below 120°. The torsion angle Cu–N_{am}–C^α–C^β defines the border between the axial and equatorial position of C^β: if the value is below –120°, C^β is in an equatorial position, else, in an axial position. These are denoted as "e" and "a" in the conformer names, followed by a two-digit index, which indicates the orientation of the imidazole ring. The first torsion angle, which is part of this orientation, N_{am}–C^α–C^β–C^γ is divided into three ranges (0° to 90°, –90° to 0° and "else", indicated by the digits 1, 2 and 3, respectively). The second relevant L-His residue angle, C^α–C^β–C^γ–C^δ is divided into 9 ranges from 0° to ±180°, indicated by one digit as listed in Table 3.

Table 3: Chosen ranges for the torsion angle C^α–C^β–C^γ–C^δ, which defines the optimized imidazole ring orientation.

C^α–C^β–C^γ–C^δ	2nd digit in conformer symbol
below −130°	1
−130° to −90°	2
−90° to −60°	3
−60° to −30°	4
−30° to 0°	5
0° to 75°	6
75° to 110°	7
110° to 140°	8
above 140°	9

Altogether, 78 *cis* and 98 *trans* GGp and 64 *cis* and 53 *trans* GpGp equilibrium structures were obtained. They are listed with their energy and torsion angle values in Table 4 (GGp) and Table 5 (GpGp). Conformers, which led to the same symbol, but had noticeable different torsion angles and electronic energy were discerned by letters A and B at the end of the symbol.

3.1.2. HISTAMINE-LIKE MODE (H MODE)

In the case of the *trans* position the valence angle N_{am}–Cu–N_{am}' is above 140° and in the *cis* position below 120°. The optimization resulted in four possible orientations of the torsion angle Cu–N_{am}–C^α–C^β including axial and equatorial position of the carboxylate group relative to the plane around copper(II): *a2* (−180° to −50°), *a1* (−50° to 0°), *e1* (0° to 50°) and *e2* (50° to 180°). A total of 22 *cis* and 10 *trans* stable equilibrium structures were obtained, which are listed with their corresponding electronic energy and torsion angles in Table 6. Only a small number of equilibrium structures is obtained in this mode, because a significant number of starting geometries developed into another configuration during the optimization (51 changed to the IGp and 60 to the GGp mode).

Table 4: List of the optimized GGp geometries with the related torsion angles, electronic energy as well as the relative electronic energy. The reference value is the electronic energy of tGGp_a19_e12 (–1292.77081 a.u.).

symbol	electronic energy [a.u.]	rel. energy [kJ mol^{-1}]	Cu–N$_{am}$–C$^{\alpha}$–C$^{\beta}$ [°]	Cu–N$_{am}$'–C$^{\alpha'}$–C$^{\beta'}$ [°]	N$_{am}$–C$^{\alpha}$–C$^{\beta}$–C$^{\gamma}$ [°]	N$_{am}$'–C$^{\alpha'}$–C$^{\beta'}$–C$^{\gamma'}$ [°]	C$^{\alpha}$–C$^{\beta}$–C$^{\gamma}$–C$^{\delta}$ [°]	C$^{\alpha'}$–C$^{\beta'}$–C$^{\gamma'}$–C$^{\delta'}$ [°]
tGGp_a19_e12	–1292.77081	0.00	–88.9	–144.1	65.3	63.3	153.1	–104.8
tGGp_a17_e12	–1292.76942	3.66	–100.7	–142.3	42.8	64.4	97.1	–98.2
tGGp_e18_e12	–1292.76843	6.27	–145.0	–155.3	58.3	61.0	119.0	–107.8
tGGp_a22_e12	–1292.76646	11.42	–99.7	–156.1	–61.9	60.4	–122.8	–108.2
tGGp_e18_e38	–1292.76555	13.82	–146.4	–154.9	58.0	–155.3	121.0	122.2
tGGp_e21_e12	–1292.76531	14.45	–158.4	–155.4	–69.2	60.3	–144.1	–107.7
tGGp_a22_e38	–1292.76377	18.50	–99.8	–155.7	–61.9	–155.2	–122.7	121.9
tGGp_e18_a38	–1292.76361	18.92	–145.1	–96.9	58.3	–156.1	120.2	134.9
tGGp_a19_e38	–1292.76354	19.09	–90.4	–158.0	62.5	–155.7	161.3	121.8
tGGp_a13_e12	–1292.76296	20.63	–87.8	–145.9	65.1	63.8	–82.8	–99.3
tGGp_e21_e38	–1292.76283	20.97	–158.6	–156.0	–69.2	–155.6	–143.7	121.3
tGGp_e21_a12	–1292.76271	21.28	–155.3	–84.1	–69.9	71.8	–145.6	–94.4
tGGp_e18_a22	–1292.76268	21.36	–145.7	–73.0	58.6	–49.6	122.0	–98.9
tGGp_a22_a12	–1292.76266	21.42	–95.4	–98.5	–64.2	66.3	–123.4	–104.7
tGGp_a22_a38	–1292.76196	23.26	–99.5	–98.2	–61.7	–155.9	–122.7	134.5
tGGp_a19_a38	–1292.76169	23.95	–90.3	–107.3	64.1	–153.5	158.1	133.0
tGGp_a28_e12	–1292.76168	23.97	–101.1	–155.1	–58.0	60.7	130.4	–107.3
tGGp_a17_e16	–1292.76116	25.34	–108.6	–132.8	42.7	51.7	91.0	32.7
tGGp_e21_a38	–1292.76067	26.64	–158.1	–100.1	–69.0	–155.4	–144.4	134.1
tGGp_e21_a22	–1292.76042	27.28	–158.8	–74.4	–68.8	–49.4	–149.1	–97.3
tGGp_a22_a22	–1292.75996	28.51	–100.3	–73.7	–62.6	–49.7	–124.7	–98.7
tGGp_e18_a27	–1292.75977	29.00	–145.7	–96.8	58.4	–62.9	118.8	101.2
tGGp_a28_a12	–1292.75953	29.62	–95.0	–98.4	–56.9	75.1	126.5	–104.8
tGGp_a19_e16	–1292.75952	29.65	–90.7	–145.3	62.2	51.3	162.2	65.7
tGGp_e18_a18	–1292.75948	29.75	–142.4	–90.7	54.6	63.9	119.0	113.9
tGGp_e18_e27	–1292.75911	30.74	–146.4	–149.3	58.6	–65.7	119.1	98.4
tGGp_a28_e38	–1292.75882	31.48	–102.1	–155.3	–58.2	–155.3	132.7	121.5
tGGp_e33_e12	–1292.75871	31.77	–159.3	–155.2	–150.9	60.4	–81.5	–107.6
tGGp_a22_a27	–1292.75799	33.68	–99.9	–97.8	–62.1	–63.1	–122.1	101.4
tGGp_e18_e16	–1292.75773	34.36	–143.8	–152.1	57.7	49.3	118.5	57.4
tGGp_e21_a16	–1292.75751	34.93	–157.7	–83.3	–70.1	55.1	–147.9	73.5
tGGp_a22_e27	–1292.75728	35.53	–100.4	–149.6	–62.1	–65.8	–121.8	99.1

Table 4 *(continued).*

symbol	electronic energy [a.u.]	rel. energy [kJ mol^{-1}]	Cu–N$_{am}$–C$^\alpha$–C$^\beta$ [°]	Cu–N$_{am}$'–C$^{\alpha'}$–C$^{\beta'}$ [°]	N$_{am}$–C$^\alpha$–C$^\beta$–C$^\gamma$ [°]	N$_{am}$'–C$^{\alpha'}$–C$^{\beta'}$–C$^{\gamma'}$ [°]	C$^\alpha$–C$^\beta$–C$^\gamma$–C$^\delta$ [°]	C$^{\alpha'}$–C$^{\beta'}$–C$^{\gamma'}$–C$^{\delta'}$ [°]
tGGp_e18_e25	−1292.75709	36.04	−145.6	−152.7	58.3	−63.7	119.3	−23.1
tGGp_a32_e12	−1292.75701	36.24	−91.5	−154.4	−166.5	60.0	−102.7	−106.9
tGGp_a28_a38	−1292.75694	36.42	−99.9	−99.7	−57.8	−155.3	131.2	134.0
tGGp_e21_a27	−1292.75676	36.91	−158.0	−98.2	−69.4	−63.2	−143.1	101.6
tGGp_a34_e12	−1292.75674	36.96	−89.4	−154.6	−162.5	60.2	−43.7	−107.2
tGGp_e18_e24	−1292.75673	36.99	−147.0	−153.5	58.1	−59.2	121.1	−53.7
tGGp_e18_a25	−1292.75671	37.03	−148.5	−99.6	58.6	−62.3	120.2	−27.0
tGGp_a19_a27	−1292.75655	37.46	−90.3	−104.4	65.7	−61.9	152.2	101.8
tGGp_e33_a12	−1292.75645	37.73	−157.8	−83.7	−151.2	72.8	−80.7	−92.8
tGGp_a19_e27	−1292.75636	37.94	−90.7	−150.7	63.5	−65.4	158.1	100.0
tGGp_e21_e27	−1292.75627	38.18	−158.0	−149.2	−69.2	−66.0	−144.1	97.4
tGGp_a11_a23	−1292.75619	38.39	−115.2	−78.9	44.8	−42.2	−138.1	−85.7
tGGp_e33_e38	−1292.75593	39.09	−159.2	−156.0	−151.1	−155.2	−82.1	120.9
tGGp_a22_a16	−1292.75592	39.09	−101.0	−92.7	−62.8	49.0	−124.1	68.0
tGGp_a22_e16	−1292.75575	39.56	−99.6	−153.7	−62.2	49.4	−122.9	58.7
cGGp_a18_a12	−1292.75537	40.55	−83.1	−88.2	72.4	44.9	130.0	−110.7
tGGp_a22_e25	−1292.75536	40.57	−100.7	−152.4	−62.1	−63.9	−121.4	−23.6
tGGp_a22_a24	−1292.75523	40.91	−101.9	−97.0	−61.6	−61.4	−120.1	−30.6
tGGp_e21_e16	−1292.75470	42.30	−157.6	−151.0	−69.2	50.0	−143.7	59.4
tGGp_a28_a16	−1292.75452	42.79	−98.4	−95.0	−53.9	56.4	119.5	67.8
tGGp_e21_e25	−1292.75446	42.95	−158.5	−153.4	−69.4	−63.8	−143.3	−26.0
tGGp_a19_e25	−1292.75407	43.95	−90.8	−156.6	63.4	−65.2	159.2	−18.8
cGGp_a18_e12	−1292.75398	44.19	−84.6	−157.7	72.6	59.8	127.7	−108.4
tGGp_a32_e38	−1292.75397	44.22	−91.7	−155.6	−166.0	−155.5	−103.4	121.3
tGGp_a34_e38	−1292.75395	44.27	−89.0	−155.9	−163.5	−155.1	−36.7	121.2
tGGp_e33_a38	−1292.75374	44.82	−158.2	−101.9	−150.7	−154.9	−80.2	133.0
tGGp_a13_e16	−1292.75371	44.92	−89.4	−145.6	62.8	53.8	−78.5	62.3
cGGp_a22_e12	−1292.75341	45.69	−85.3	−156.1	−60.0	58.6	−121.5	−107.7
tGGp_e33_a22	−1292.75321	46.23	−159.0	−74.1	−151.6	−49.1	−87.8	−97.1
tGGp_a28_a27	−1292.75320	46.25	−100.8	−99.2	−58.5	−63.0	128.5	101.7
tGGp_a32_a12	−1292.75314	46.39	−87.9	−107.3	−168.2	65.4	−112.6	−104.5
cGGp_e18_e12	−1292.75311	46.49	−146.0	−156.6	58.4	58.7	118.3	−107.7
tGGp_a37_a23	−1292.75295	46.89	−79.8	−83.4	158.2	−50.8	81.4	−71.5

Table 4 (continued).

symbol	electronic energy [a.u.]	rel. energy [kJ mol^{-1}]	Cu–N$_{am}$–C$^\alpha$–C$^\beta$ [°]	Cu–N$_{am}$'–C$^{\alpha'}$–C$^{\beta'}$ [°]	N$_{am}$–C$^\alpha$–C$^\beta$–C$^\gamma$ [°]	N$_{am}$'–C$^{\alpha'}$–C$^{\beta'}$–C$^{\gamma'}$ [°]	C$^\alpha$–C$^\beta$–C$^\gamma$–C$^\delta$ [°]	C$^{\alpha'}$–C$^{\beta'}$–C$^{\gamma'}$–C$^{\delta'}$ [°]
tGGp_a28_e27	−1292.75262	47.78	−101.4	−149.7	−58.7	−65.4	128.9	98.4
cGGp_a22_a12	−1292.75259	47.85	−92.4	−85.9	−62.5	47.0	−122.2	−111.6
tGGp_a32_a38	−1292.75205	49.27	−92.5	−98.7	−165.2	−155.3	−103.9	133.7
tGGp_e18_e33	−1292.75175	50.04	−146.8	−161.0	58.4	−150.4	120.4	−68.4
tGGp_a28_e16	−1292.75168	50.23	−96.4	−149.7	−57.3	50.7	124.3	60.7
cGGp_e18_a12	−1292.75155	50.59	−142.0	−88.0	57.3	48.7	115.0	−112.9
tGGp_e33_a16	−1292.75150	50.71	−159.4	−82.8	−152.1	56.2	−80.6	73.0
cGGp_e21_e12	−1292.75134	51.12	−164.0	−156.4	−67.7	58.8	−140.8	−107.6
cGGp_a18_e38	−1292.75113	51.69	−85.4	−161.1	70.8	−154.5	132.5	121.2
tGGp_a28_e25	−1292.75077	52.62	−100.1	−152.9	−58.4	−63.7	127.0	−25.5
tGGp_a32_a22	−1292.75068	52.85	−93.6	−73.8	−166.1	−49.1	−110.8	−99.0
tGGp_a36_e38	−1292.75067	52.89	−88.2	−154.9	174.2	−155.1	60.8	121.1
tGGp_e33_a27	−1292.75037	53.68	−159.2	−97.3	−151.2	−62.9	−79.2	100.1
cGGp_a18_a38	−1292.75026	53.95	−84.6	−90.8	71.7	−157.8	126.9	136.6
tGGp_a22_e33	−1292.75012	54.34	−100.5	−161.2	−61.9	−150.2	−122.3	−68.0
tGGp_e33_e27	−1292.74984	55.06	−158.9	−150.0	−151.3	−66.8	−80.2	96.1
cGGp_a22_e38	−1292.74971	55.42	−84.7	−160.1	−60.0	−156.0	−123.1	121.3
cGGp_a17_e38	−1292.74957	55.79	−96.4	−162.9	57.2	−155.0	105.5	118.6
cGGp_e18_e38	−1292.74955	55.82	−143.6	−161.0	57.8	−155.9	117.5	120.9
tGGp_a19_e33	−1292.74954	55.86	−90.5	−163.9	61.9	−151.7	162.7	−71.6
tGGp_e21_e33	−1292.74913	56.93	−158.2	−160.5	−69.4	−150.5	−143.8	−68.8
cGGp_e21_a12	−1292.74893	57.44	−163.1	−87.4	−67.2	49.1	−137.5	−116.0
tGGp_a34_a27	−1292.74869	58.08	−88.8	−97.8	−163.9	−62.3	−37.6	100.7
tGGp_a32_a27	−1292.74862	58.27	−91.9	−97.7	−166.0	−62.2	−102.0	100.9
tGGp_a36_a38	−1292.74849	58.61	−88.5	−105.6	173.0	−153.9	68.1	132.0
tGGp_e33_e16	−1292.74828	59.16	−159.2	−153.1	−150.9	49.5	−80.2	60.2
tGGp_e33_e25	−1292.74807	59.72	−159.2	−153.6	−151.2	−63.6	−79.4	−24.7
tGGp_a34_e27	−1292.74803	59.82	−88.5	−149.8	−164.1	−64.9	−36.5	98.2
tGGp_a37_a12	−1292.74796	60.01	−93.3	−94.7	171.3	73.2	79.6	−100.6
tGGp_a32_e27	−1292.74795	60.03	−91.8	−150.2	−166.4	−65.1	−101.1	98.1
tGGp_e33_a24	−1292.74776	60.52	−159.6	−95.8	−151.4	−60.2	−78.8	−38.8
cGGp_e21_e38	−1292.74775	60.56	−162.8	−158.6	−67.5	−155.7	−143.5	121.9
cGGp_a22_a38	−1292.74746	61.32	−89.1	−92.0	−61.7	−157.0	−124.6	135.4

Table 4 (continued).

symbol	electronic energy [a.u.]	rel. energy [kJ mol⁻¹]	Cu–N$_{am}$–C$^\alpha$–C$^\beta$ [°]	Cu–N$_{am}$'–C$^{\alpha'}$–C$^{\beta'}$ [°]	N$_{am}$–C$^\alpha$–C$^\beta$–C$^\gamma$ [°]	N$_{am}$'–C$^{\alpha'}$–C$^{\beta'}$–C$^{\gamma'}$ [°]	C$^\alpha$–C$^\beta$–C$^\gamma$–C$^\delta$ [°]	C$^{\alpha'}$–C$^{\beta'}$–C$^{\gamma'}$–C$^{\delta'}$ [°]
cGGp_e18_a38	−1292.74744	61.36	−143.9	−90.1	58.2	−156.7	117.7	135.2
cGGp_a18_a27	−1292.74726	61.83	−85.0	−91.4	71.4	−60.0	125.8	99.9
tGGp_a32_e16	−1292.74651	63.80	−92.6	−152.7	−166.4	49.0	−103.6	58.7
tGGp_a34_e16	−1292.74632	64.32	−89.3	−152.0	−163.1	49.2	−41.0	58.1
tGGp_a32_a16	−1292.74630	64.37	−109.0	−90.0	−163.3	49.8	−114.4	70.3
tGGp_a34_e25	−1292.74625	64.50	−88.4	−152.4	−164.0	−62.8	−36.5	−26.0
tGGp_a34_a24	−1292.74614	64.77	−88.2	−97.1	−164.6	−61.0	−33.9	−30.5
tGGp_a32_e25	−1292.74605	65.02	−92.0	−152.9	−165.6	−63.7	−100.4	−23.5
cGGp_e21_a38	−1292.74589	65.44	−163.5	−89.9	−67.5	−156.7	−142.4	135.1
tGGp_a32_a25	−1292.74571	65.90	−92.2	−99.6	−165.0	−62.0	−98.6	−25.6
cGGp_a22_e27	−1292.74568	65.99	−74.6	−161.9	−49.7	−62.9	−108.9	91.0
tGGp_a28_e33	−1292.74565	66.08	−101.7	−161.1	−58.2	−150.6	128.1	−68.5
tGGp_a32_a24	−1292.74561	66.17	−92.5	−97.2	−165.0	−60.2	−95.2	−36.3
tGGp_a37_a17	−1292.74528	67.05	−98.9	−90.2	169.1	64.3	80.7	107.4
cGGp_a18_e27	−1292.74515	67.38	−84.8	−157.2	71.9	−64.7	128.1	93.1
cGGp_a18_a24	−1292.74490	68.03	−85.0	−86.2	70.4	−56.4	129.0	−31.0
cGGp_e18_a27	−1292.74461	68.79	−145.4	−91.7	58.5	−59.5	117.7	99.7
cGGp_a22_a27	−1292.74458	68.87	−88.5	−93.7	−61.8	−60.3	−124.0	99.7
cGGp_a22_e25	−1292.74380	70.93	−74.4	−158.2	−50.6	−58.8	−110.6	−22.4
cGGp_a18_e25	−1292.74359	71.47	−85.0	−160.9	71.6	−62.1	129.1	−25.5
cGGp_e18_e27	−1292.74350	71.71	−144.3	−157.8	58.3	−64.9	117.0	93.3
cGGp_e21_a27	−1292.74322	72.44	−164.0	−90.6	−67.8	−60.1	−142.3	98.6
tGGp_a36_e16	−1292.74264	73.97	−90.3	−152.5	175.3	50.8	68.4	63.6
tGGp_e33_e33	−1292.74255	74.22	−158.3	−160.0	−150.8	−150.2	−79.4	−67.3
cGGp_e33_e12	−1292.74236	74.70	−162.9	−157.1	−151.2	58.6	−77.4	−107.4
cGGp_e21_e27	−1292.74214	75.29	−162.4	−157.2	−67.6	−65.0	−143.2	93.3
cGGp_a22_a25	−1292.74193	75.82	−88.4	−90.8	−62.0	−57.8	−124.7	−24.9
cGGp_e18_a25	−1292.74188	75.98	−143.1	−88.7	58.6	−57.1	116.3	−26.8
cGGp_a18_a16	−1292.74185	76.05	−83.4	−94.3	74.3	35.4	121.9	60.8
cGGp_e18_e25	−1292.74178	76.22	−143.1	−159.5	57.7	−60.7	116.8	−26.4
cGGp_a18_e16	−1292.74147	77.05	−84.4	−153.9	72.4	49.2	125.6	36.6
cGGp_a34_a12	−1292.74143	77.14	−85.4	−85.3	−163.6	46.5	−39.6	−108.7
cGGp_a22_a16	−1292.74124	77.64	−91.9	−93.3	−62.7	43.2	−121.8	59.3

19

Table 4 (continued).

symbol	electronic energy [a.u.]	rel. energy [kJ mol^{-1}]	Cu–N$_{am}$–C$^{\alpha}$–C$^{\beta}$ [°]	Cu–N$_{am}$'–C$^{\alpha}$'–C$^{\beta}$' [°]	N$_{am}$–C$^{\alpha}$–C$^{\beta}$–C$^{\gamma}$ [°]	N$_{am}$'–C$^{\alpha}$'–C$^{\beta}$'–C$^{\gamma}$' [°]	C$^{\alpha}$–C$^{\beta}$–C$^{\gamma}$–C$^{\delta}$ [°]	C$^{\alpha}$'–C$^{\beta}$'–C$^{\gamma}$'–C$^{\delta}$' [°]
cGGp_a34_e12	−1292.74102	78.24	−82.2	−155.6	−163.3	58.5	−42.2	−106.8
cGGp_e18_a16	−1292.74096	78.39	−149.6	−92.2	58.3	43.3	115.3	61.2
tGGp_a34_e33	−1292.74067	79.15	−89.2	−160.8	−163.2	−150.3	−37.2	−70.4
tGGp_a32_e33	−1292.74065	79.20	−92.7	−160.8	−165.8	−150.8	−102.4	−70.3
cGGp_a22_e16	−1292.74065	79.21	−85.9	−155.1	−61.1	46.9	−121.1	47.9
cGGp_a18_e24	−1292.74056	79.43	−112.9	−167.2	49.2	−62.8	114.9	−46.5
cGGp_a33_a12	−1292.74049	79.62	−85.8	−84.8	−164.9	44.3	−84.6	−108.2
cGGp_e18_e16	−1292.74036	79.96	−145.3	−155.2	58.5	47.1	116.5	46.3
cGGp_e21_a25	−1292.74020	80.38	−162.5	−89.0	−67.7	−57.9	−143.4	−26.7
cGGp_e21_e25	−1292.74009	80.66	−162.4	−158.0	−67.6	−60.7	−143.3	−26.5
cGGp_e33_a12	−1292.73958	82.01	−159.9	−86.0	−149.4	52.2	−72.6	−113.3
cGGp_e21_e16	−1292.73866	84.43	−164.1	−155.1	−68.0	46.8	−139.2	48.7
cGGp_e33_e38	−1292.73849	84.87	−162.7	−160.4	−150.9	−155.9	−79.9	120.8
cGGp_e21_a16	−1292.73829	85.39	−163.0	−90.3	−67.5	46.1	−136.5	60.8
tGGp_a36_e33	−1292.73721	88.22	−87.5	−160.1	172.9	−150.6	66.0	−68.0
cGGp_a34_e38	−1292.73673	89.48	−83.0	−159.1	−163.1	−155.6	−53.7	121.0
cGGp_a32_e38	−1292.73672	89.50	−83.7	−159.8	−164.3	−155.6	−94.0	120.9
cGGp_e33_a38	−1292.73639	90.37	−162.7	−89.9	−150.1	−156.7	−81.7	134.8
cGGp_a18_e33	−1292.73623	90.79	−84.8	−166.2	71.2	−148.7	128.6	−64.3
cGGp_a34_a38	−1292.73487	94.38	−82.0	−90.5	−164.0	−156.9	−45.9	134.9
cGGp_a32_a38	−1292.73475	94.69	−83.6	−89.6	−166.0	−157.2	−94.2	135.3
cGGp_a17_e34	−1292.73449	95.38	−94.0	−163.6	58.5	−146.7	100.6	−59.2
cGGp_a22_e33	−1292.73426	95.98	−85.7	−163.6	−60.9	−152.0	−121.8	−67.8
cGGp_e18_e33	−1292.73411	96.38	−143.7	−163.9	58.2	−151.2	115.6	−64.3
cGGp_e33_a27	−1292.73409	96.43	−163.3	−92.4	−150.8	−59.7	−79.7	99.4
cGGp_e33_e27	−1292.73333	98.41	−163.5	−158.4	−151.7	−64.8	−79.6	92.1
cGGp_a34_a27	−1292.73282	99.76	−82.3	−92.8	−164.0	−59.4	−43.1	99.6
cGGp_a32_a27	−1292.73256	100.44	−82.7	−91.5	−166.9	−59.1	−91.6	99.2
cGGp_e21_e33	−1292.73227	101.19	−163.1	−162.7	−67.8	−150.8	−141.7	−64.7
cGGp_a34_e27	−1292.73191	102.15	−82.3	−158.7	−163.4	−63.5	−42.0	93.7
cGGp_e33_e25	−1292.73149	103.24	−163.0	−159.4	−150.8	−59.3	−78.9	−28.7
cGGp_e33_a25	−1292.73145	103.34	−164.0	−89.0	−151.3	−57.2	−82.0	−27.6
cGGp_e33_a16	−1292.73070	105.32	−162.1	−89.7	−150.9	46.7	−71.9	59.7

Table 4 *(continued).*

symbol	electronic energy [a.u.]	rel. energy [kJ mol^{-1}]	Cu–N$_{am}$–C$^\alpha$–C$^\beta$ [°]	Cu–N$_{am}$'–C$^{\alpha'}$–C$^{\beta'}$ [°]	N$_{am}$–C$^\alpha$–C$^\beta$–C$^\gamma$ [°]	N$_{am}$'–C$^{\alpha'}$–C$^{\beta'}$–C$^{\gamma'}$ [°]	C$^\alpha$–C$^\beta$–C$^\gamma$–C$^\delta$ [°]	C$^{\alpha'}$–C$^{\beta'}$–C$^{\gamma'}$–C$^{\delta'}$ [°]
cGGp_a34_a16	−1292.73039	106.13	−86.6	−92.4	−161.0	42.6	−44.6	58.5
cGGp_e33_e16	−1292.73010	106.89	−163.7	−153.6	−151.5	47.1	−75.6	44.2
cGGp_a32_a24	−1292.73007	106.98	−82.7	−86.3	−168.1	−56.1	−95.5	−30.2
cGGp_a34_a25	−1292.73005	107.02	−82.7	−88.5	−164.4	−56.8	−50.6	−27.6
cGGp_a34_e25	−1292.72991	107.38	−82.3	−159.5	−163.7	−59.8	−47.8	−27.0
cGGp_a33_e25	−1292.72984	107.58	−83.2	−159.2	−166.0	−60.3	−89.7	−28.0
cGGp_a13_a27	−1292.72965	108.06	−82.2	−94.2	65.3	−58.8	−88.7	99.0
cGGp_a34_e16	−1292.72879	110.34	−81.9	−153.6	−163.1	47.3	−43.0	44.5
cGGp_a13_a24	−1292.72792	112.61	−82.2	−89.6	64.8	−56.1	−88.3	−34.2
cGGp_e33_e33	−1292.72347	124.30	−163.6	−163.1	−150.9	−151.5	−78.2	−65.9
cGGp_e33_a35	−1292.72235	127.25	−164.0	−80.7	−150.7	−164.0	−81.7	−19.1
cGGp_a34_e33	−1292.72195	128.28	−81.6	−163.7	−163.3	−151.3	−47.1	−66.5

Table 5: List of the optimized GpGp geometries with the related torsion angles, electronic energy as well as the relative electronic energy.
The reference value is the electronic energy of tGGp_a19_e12 (−1292.77081 a.u.).

symbol	electronic energy [a.u.]	rel. energy [kJ mol^{-1}]	Cu–N$_{am}$–C$^\alpha$–C$^\beta$ [°]	Cu–N$_{am}$'–C$^{\alpha'}$–C$^{\beta'}$ [°]	N$_{am}$–C$^\alpha$–C$^\beta$–C$^\gamma$ [°]	N$_{am}$'–C$^{\alpha'}$–C$^{\beta'}$–C$^{\gamma'}$ [°]	C$^\alpha$–C$^\beta$–C$^\gamma$–C$^\delta$ [°]	C$^{\alpha'}$–C$^{\beta'}$–C$^{\gamma'}$–C$^{\delta'}$ [°]
tGpGp_e12_e12_A	−1292.76632	11.80	−155.5	−155.5	60.2	60.2	−107.1	−107.1
tGpGp_e12_e38	−1292.76346	19.31	−154.4	−155.8	60.1	−155.1	−106.5	120.9
tGpGp_e12_e12_B	−1292.76245	21.96	−129.7	−129.7	57.2	57.1	−104.5	−104.5
tGpGp_a12_e38	−1292.76239	22.10	−83.9	−154.4	72.4	−154.9	−90.9	121.1
tGpGp_a12_a23	−1292.76217	22.70	−91.1	−98.0	76.8	−57.8	−98.6	−68.3
tGpGp_e38_e38	−1292.76030	27.61	−154.5	−154.5	−154.9	−154.9	120.8	120.8
tGpGp_a27_e12	−1292.75843	32.51	−98.1	−154.6	−61.5	59.9	100.3	−106.8
tGpGp_a38_e38	−1292.75805	33.51	−102.6	−155.4	−154.7	−155.1	132.5	120.6
tGpGp_e12_e27	−1292.75777	34.25	−153.6	−148.9	60.3	−65.0	−106.6	97.0
tGpGp_a16_a23	−1292.75739	35.25	−94.5	−96.3	55.7	−51.8	61.4	−67.7
tGpGp_a16_e12	−1292.75735	35.36	−85.4	−151.9	59.3	68.9	70.0	−107.1
tGpGp_a16_e38	−1292.75719	35.78	−83.3	−156.9	55.1	−156.0	70.5	120.2
tGpGp_a12_e27	−1292.75683	36.71	−83.8	−147.6	72.5	−66.2	−92.9	96.3
tGpGp_e12_e25	−1292.75605	38.77	−153.1	−150.7	60.3	−62.3	−106.3	−28.3
tGpGp_e12_e16	−1292.75601	38.86	−155.3	−152.0	60.2	49.6	−107.4	54.0
tGpGp_a24_e12	−1292.75601	38.87	−96.8	−154.0	−60.8	60.5	−30.2	−106.2
tGpGp_a12_e17	−1292.75568	39.72	−85.3	−138.9	75.4	76.9	−93.1	107.2
tGpGp_a27_e38	−1292.75539	40.50	−97.6	−155.1	−61.9	−155.1	99.9	121.2
tGpGp_e27_e38	−1292.75482	42.00	−149.0	−154.9	−65.6	−155.2	96.9	120.9
tGpGp_e16_e38	−1292.75355	45.32	−150.3	−154.5	49.6	−155.0	57.2	121.6
tGpGp_e25_e38	−1292.75304	46.67	−153.3	−155.3	−62.9	−155.3	−25.9	120.8
tGpGp_a24_e38	−1292.75267	47.64	−96.8	−155.1	−60.3	−155.3	−34.4	121.2
tGpGp_a38_e27	−1292.75263	47.74	−102.3	−149.1	−154.6	−65.5	132.7	96.5
cGpGp_a12_a12	−1292.75132	51.19	−86.6	−86.6	49.7	49.7	−106.5	−106.5
tGpGp_a16_e27	−1292.75129	51.25	−83.2	−152.2	55.0	−66.5	71.2	95.7
cGpGp_e12_e12	−1292.75126	51.35	−155.2	−155.1	58.2	58.2	−106.1	−106.1
tGpGp_a38_e25	−1292.75091	52.25	−102.3	−152.1	−154.6	−62.7	132.7	−26.5
tGpGp_a25_a38	−1292.75070	52.80	−98.2	−99.5	−60.9	−155.3	−29.6	133.7
tGpGp_a16_e17	−1292.75070	52.81	−84.6	−153.4	58.3	58.7	71.1	75.4
cGpGp_a12_e12	−1292.75063	53.01	−94.4	−153.0	54.9	58.8	−106.9	−106.0
tGpGp_e12_e33	−1292.75032	53.80	−154.7	−160.5	60.5	−150.0	−107.0	−69.1
tGpGp_a27_a27	−1292.75020	54.13	−99.6	−99.6	−62.4	−62.4	101.4	101.4
tGpGp_a16_a27	−1292.74977	55.24	−89.5	−107.1	50.9	−60.5	66.4	106.1
tGpGp_a27_e27	−1292.74946	56.08	−97.1	−147.6	−62.7	−65.5	99.7	98.4

Table 5 (continued).

symbol	electronic energy [a.u.]	rel. energy [kJ mol^{-1}]	Cu–N$_{am}$–C$^\alpha$–C$^\beta$ [°]	Cu–N$_{am}$'–C$^{\alpha'}$–C$^{\beta'}$ [°]	N$_{am}$–C$^\alpha$–C$^\beta$–C$^\gamma$ [°]	N$_{am}$'–C$^{\alpha'}$–C$^{\beta'}$–C$^{\gamma'}$ [°]	C$^\alpha$–C$^\beta$–C$^\gamma$–C$^\delta$ [°]	C$^{\alpha'}$–C$^{\beta'}$–C$^{\gamma'}$–C$^{\delta'}$ [°]
tGpGp_e27_e27	–1292.74904	57.18	–149.1	–149.1	–66.2	–66.2	96.5	96.5
tGpGp_a12_e33	–1292.74902	57.23	–83.8	–156.6	72.9	–148.6	–91.9	–64.4
tGpGp_a27_e16	–1292.74814	59.53	–98.9	–152.0	–62.5	49.0	101.4	58.4
tGpGp_a27_e25	–1292.74777	60.49	–98.7	–152.6	–62.5	–63.5	101.1	–24.3
tGpGp_e16_e27	–1292.74755	61.09	–151.1	–148.9	49.5	–66.7	60.5	96.5
tGpGp_a25_a27	–1292.74746	61.33	–100.0	–99.1	–61.9	–62.4	–25.4	101.1
tGpGp_e33_e38	–1292.74742	61.43	–160.3	–155.4	–150.5	–155.1	–69.4	120.9
tGpGp_e25_e27	–1292.74726	61.85	–151.8	–149.2	–62.8	–65.5	–25.3	97.1
tGpGp_a25_e27	–1292.74685	62.92	–99.5	–150.2	–62.1	–65.3	–28.3	97.6
cGpGp_e12_e38	–1292.74662	63.51	–155.9	–159.7	57.9	–156.4	–106.0	120.9
cGpGp_a12_e28	–1292.74632	64.30	–94.9	–173.3	64.8	–57.0	–107.7	129.9
tGpGp_e16_e16	–1292.74592	65.36	–152.3	–152.2	50.8	50.8	60.1	60.1
tGpGp_e16_e25	–1292.74591	65.39	–150.5	–151.8	49.8	–62.7	60.3	–28.5
cGpGp_a12_a38	–1292.74575	65.81	–86.0	–93.4	47.7	–157.0	–108.0	135.0
cGpGp_a12_e38	–1292.74542	66.67	–97.3	–156.8	54.5	–156.6	–104.5	121.1
tGpGp_e25_e25	–1292.74539	66.76	–151.2	–151.2	–62.7	–62.7	–26.6	–26.6
tGpGp_a38_e33	–1292.74522	67.19	–101.6	–159.6	–154.9	–150.4	132.9	–69.4
tGpGp_a25_e25	–1292.74501	67.75	–99.5	–153.3	–61.9	–63.6	–28.3	–24.1
tGpGp_a16_e33	–1292.74472	68.50	–82.5	–159.5	56.5	–151.5	73.1	–69.4
cGpGp_a38_e12	–1292.74468	68.61	–89.1	–155.5	–157.2	57.8	135.2	–106.2
tGpGp_a22_e33	–1292.74441	69.32	–74.1	–159.7	–49.1	–151.5	–96.7	–70.6
tGpGp_a25_a25	–1292.74441	69.33	–102.2	–102.2	–62.6	–62.6	–21.8	–21.7
cGpGp_a12_a27	–1292.74398	70.45	–86.2	–94.6	47.5	–58.4	–108.9	101.2
cGpGp_a27_e12	–1292.74299	73.05	–92.7	–155.8	–58.0	58.4	100.0	–106.7
cGpGp_e38_e38	–1292.74237	74.69	–159.6	–159.6	–155.5	–155.5	120.6	120.6
tGpGp_a27_e33	–1292.74220	75.11	–97.8	–160.5	–62.5	–150.2	100.0	–67.6
cGpGp_e12_e27	–1292.74191	75.88	–155.2	–158.4	58.6	–62.9	–106.2	94.1
tGpGp_e27_e33	–1292.74158	76.76	–148.3	–159.8	–65.9	–150.0	96.8	–69.0
cGpGp_a12_a16	–1292.74152	76.91	–89.5	–91.3	53.3	40.8	–107.5	58.7
cGpGp_a16_e12	–1292.74123	77.67	–92.7	–158.4	43.9	57.8	58.9	–106.7
cGpGp_a12_a25	–1292.74084	78.70	–86.2	–93.2	46.8	–57.8	–108.7	–23.1
tGpGp_e16_e33	–1292.74041	79.84	–152.1	–160.2	49.7	–149.6	60.3	–68.0
cGpGp_a38_e38	–1292.74009	80.67	–91.0	–159.4	–156.3	–155.6	133.9	120.8
cGpGp_a25_e12	–1292.73990	81.18	–90.2	–155.4	–57.4	58.5	–24.3	–106.8
cGpGp_e12_e25	–1292.73985	81.29	–155.4	–159.0	58.6	–59.1	–106.9	–27.3

Table 5 (continued).

symbol	electronic energy [a.u.]	rel. energy [kJ mol^{-1}]	Cu–N$_{am}$–C$^\alpha$–C$^\beta$ [°]	Cu–N$_{am}$'–C$^{\alpha'}$–C$^{\beta'}$ [°]	N$_{am}$–C$^\alpha$–C$^\beta$–C$^\gamma$ [°]	N$_{am}$'–C$^{\alpha'}$–C$^{\beta'}$–C$^{\gamma'}$ [°]	C$^\alpha$–C$^\beta$–C$^\gamma$–C$^\delta$ [°]	C$^{\alpha'}$–C$^{\beta'}$–C$^{\gamma'}$–C$^{\delta'}$ [°]
tGpGp_e25_e33	–1292.73983	81.35	–153.1	–160.1	–63.5	–150.6	–25.4	–69.5
cGpGp_a12_e25	–1292.73945	82.34	–91.6	–161.3	58.3	–60.5	–106.9	–28.3
cGpGp_e12_e16	–1292.73935	82.62	–157.6	–150.9	58.2	46.7	–106.8	41.0
cGpGp_a12_e16	–1292.73907	83.36	–95.9	–148.1	54.7	46.8	–106.8	41.8
cGpGp_a27_e38	–1292.73872	84.27	–92.5	–160.1	–58.4	–155.9	98.9	120.5
cGpGp_a38_a38	–1292.73797	86.22	–90.5	–90.5	–156.8	–156.8	134.3	134.4
cGpGp_e27_e38	–1292.73787	86.48	–157.3	–159.6	–64.0	–155.7	91.0	121.0
cGpGp_a27_a38	–1292.73670	89.56	–92.4	–90.2	–58.3	–157.2	98.6	135.2
cGpGp_a25_e38	–1292.73615	91.01	–89.6	–160.5	–56.6	–155.6	–26.3	120.1
cGpGp_e25_e38	–1292.73614	91.04	–159.7	–159.2	–59.0	–155.7	–29.5	120.9
cGpGp_a16_e38	–1292.73613	91.08	–91.0	–158.4	44.1	–156.4	59.2	122.7
cGpGp_a38_e27	–1292.73586	91.77	–89.3	–159.0	–156.9	–63.6	134.9	91.8
cGpGp_a16_a38	–1292.73539	93.00	–92.2	–94.0	42.1	–156.3	58.0	134.3
cGpGp_e16_e38	–1292.73473	94.75	–153.4	–159.7	46.7	–156.2	43.4	121.4
cGpGp_a27_a27	–1292.73468	94.86	–91.7	–91.7	–58.7	–58.7	99.6	99.6
tGpGp_e33_e33	–1292.73453	95.28	–160.0	–159.9	–150.1	–150.1	–70.1	–70.1
cGpGp_a38_e25	–1292.73396	96.75	–90.5	–159.3	–156.8	–58.9	134.6	–28.8
cGpGp_a25_a38	–1292.73390	96.91	–90.2	–89.1	–56.9	–157.2	–25.3	135.0
cGpGp_a16_e27	–1292.73375	97.31	–92.7	–166.7	45.5	–64.1	63.9	100.4
cGpGp_a27_e27	–1292.73360	97.71	–92.1	–157.6	–59.0	–63.1	99.5	94.0
cGpGp_a16_a27	–1292.73330	98.49	–93.5	–95.0	41.3	–58.5	59.8	99.8
cGpGp_a38_e16	–1292.73283	99.72	–90.0	–152.8	–156.5	46.6	134.8	44.9
cGpGp_e27_e27	–1292.73282	99.75	–158.0	–158.0	–64.7	–64.7	92.6	92.6
cGpGp_e12_e33	–1292.73224	101.28	–155.7	–164.0	58.1	–152.1	–106.6	–68.3
cGpGp_a25_a27	–1292.73191	102.15	–89.9	–91.2	–57.4	–58.8	–24.8	99.4
cGpGp_a27_e25	–1292.73155	103.09	–93.1	–158.9	–60.1	–60.5	99.6	–27.4
cGpGp_a27_e16	–1292.73100	104.52	–91.7	–155.2	–58.2	46.3	99.7	48.0
cGpGp_e25_e27	–1292.73097	104.61	–159.7	–158.0	–60.4	–65.3	–27.8	92.0
cGpGp_a16_a16	–1292.73075	105.18	–93.9	–93.9	43.5	43.5	57.3	57.3
cGpGp_a25_e27	–1292.73068	105.38	–90.4	–156.3	–58.0	–64.7	–25.1	92.1
cGpGp_a16_e24	–1292.73032	106.31	–93.4	–160.4	42.1	–60.9	60.9	–32.8
cGpGp_a16_a25	–1292.73008	106.95	–93.1	–94.3	41.7	–57.8	59.4	–21.9
cGpGp_e16_e27	–1292.73005	107.01	–151.9	–160.9	46.6	–63.2	45.3	93.9
cGpGp_a24_a24	–1292.72946	108.57	–86.0	–86.0	–56.1	–56.1	–30.2	–30.3
cGpGp_e25_e25	–1292.72925	109.13	–159.5	–159.5	–60.1	–60.1	–29.1	–29.1

24

Table 5 (continued).

symbol	electronic energy [a.u.]	rel. energy [kJ mol^{-1}]	Cu–N$_{am}$–C$^{\alpha}$–C$^{\beta}$ [°]	Cu–N$_{am}$'–C$^{\alpha'}$–C$^{\beta'}$ [°]	N$_{am}$–C$^{\alpha}$–C$^{\beta}$–C$^{\gamma}$ [°]	N$_{am}$'–C$^{\alpha'}$–C$^{\beta'}$–C$^{\gamma'}$ [°]	C$^{\alpha}$–C$^{\beta}$–C$^{\gamma}$–C$^{\delta}$ [°]	C$^{\alpha'}$–C$^{\beta'}$–C$^{\gamma'}$–C$^{\delta'}$ [°]
cGpGp_a25_e25	–1292.72914	109.42	–89.8	–159.0	–57.7	–60.5	–27.0	–27.0
cGpGp_a16_e16	–1292.72860	110.83	–96.2	–155.9	42.3	46.2	58.6	43.2
cGpGp_e16_e25	–1292.72791	112.64	–152.4	–160.3	46.8	–58.5	45.3	–27.8
cGpGp_a25_e16	–1292.72784	112.82	–89.5	–154.2	–57.1	47.1	–23.6	46.0
cGpGp_e33_e38	–1292.72774	113.09	–162.8	–160.7	–151.1	–155.9	–65.5	120.5
cGpGp_e16_e16	–1292.72698	115.08	–153.8	–153.8	46.6	46.6	43.2	43.3
cGpGp_a27_e33	–1292.72424	122.29	–91.0	–163.7	–57.9	–150.8	99.1	–66.3
cGpGp_e27_e33	–1292.72318	125.06	–158.4	–163.5	–63.7	–151.3	91.1	–65.5
cGpGp_a25_e33	–1292.72147	129.55	–88.4	–162.5	–56.6	–149.2	–24.8	–62.2
cGpGp_e25_e33	–1292.72133	129.91	–160.3	–162.8	–58.8	–150.6	–28.3	–65.3
cGpGp_e16_e33	–1292.71988	133.73	–152.9	–164.5	46.6	–152.7	42.3	–68.2
cGpGp_e33_e33	–1292.71274	152.47	–163.6	–163.6	–151.9	–151.9	–66.3	–66.3

25

Table 6: List of the optimized HGp geometries with the related torsion angles, electronic energy as well as the relative electronic energy.
The reference value is the electronic energy of tGGp_a19_e12 (–1292.77081 a.u.).

symbol	electronic energy [a.u.]	rel. energy [kJ mol^{-1}]	Cu–N$_{am}$–C$^\alpha$–C$^\beta$ [°]	Cu–N$_{am}$'–C$^{\alpha'}$–C$^{\beta'}$ [°]	N$_{am}$–C$^\alpha$–C$^\beta$–C$^\gamma$ [°]	N$_{am}$'–C$^{\alpha'}$–C$^{\beta'}$–C$^{\gamma'}$ [°]	N$_{am}$–C$^\alpha$–C–O^1 [°]	C$^{\alpha'}$–C$^{\beta'}$–C$^{\gamma'}$–C$^{\delta'}$ [°]
cHGp_a2_a17	–1292.75739	35.23	–68.5	–95.1	65.5	69.0	–163.5	94.5
cHGp_a2_a12	–1292.74697	62.60	–67.9	–93.1	61.8	86.5	–158.0	–106.8
cHGp_a1_a17	–1292.74674	63.20	–42.8	–98.8	–21.0	60.2	–172.9	89.3
cHGp_e2_e12	–1292.74221	75.09	74.7	–154.7	–65.2	59.8	–161.2	–105.7
cHGp_e1_e12	–1292.74191	75.88	29.5	–156.1	–62.9	60.5	168.0	–106.4
cHGp_e1_e38	–1292.73934	82.65	25.2	–156.7	–61.4	–154.5	169.0	121.0
cHGp_e2_e38	–1292.73845	84.97	74.1	–157.5	–64.9	–155.7	–161.4	120.3
cHGp_e2_a12	–1292.73829	85.40	72.9	–92.4	–65.6	66.0	–161.3	–102.8
cHGp_e1_a38	–1292.73705	88.65	25.5	–92.5	–61.5	–155.9	168.7	134.8
cHGp_e2_a38	–1292.73656	89.93	73.4	–94.2	–65.5	–156.1	–161.3	134.6
tHGp_e1_e12	–1292.73645	90.23	24.9	–127.3	–64.4	57.3	166.0	–102.0
cHGp_e2_a16	–1292.73436	95.72	72.7	–87.7	–64.0	46.4	–161.7	64.9
cHGp_e1_a27	–1292.73407	96.46	30.8	–94.4	–62.6	–62.8	166.8	99.5
cHGp_e2_a27	–1292.73387	97.00	72.9	–96.5	–66.1	–60.7	–161.1	102.0
cHGp_e1_e27	–1292.73374	97.34	29.1	–153.1	–62.2	–66.3	167.5	93.6
cHGp_e2_e27	–1292.73303	99.21	73.4	–152.3	–65.7	–62.9	–161.7	99.0
cHGp_e2_e16	–1292.73263	100.25	75.1	–151.4	–64.9	48.7	–161.4	50.4
cHGp_e1_e16	–1292.73254	100.50	26.4	–152.6	–61.8	50.1	169.1	59.5
cHGp_e1_e24	–1292.73229	101.13	27.6	–155.8	–61.6	–61.9	167.8	–36.3
cHGp_e2_a25	–1292.73106	104.37	72.5	–95.1	–65.7	–60.7	–161.3	–27.3
cHGp_e2_e25	–1292.73105	104.41	73.0	–154.3	–65.3	–62.3	–161.8	–28.2
tHGp_e1_e38	–1292.73016	106.73	32.9	–160.9	–65.8	–156.4	163.2	120.2
tHGp_e1_a38	–1292.72893	109.96	30.0	–90.7	–65.2	–156.3	163.6	134.8
tHGp_e1_a27	–1292.72755	113.58	36.1	–91.7	–65.7	–55.0	162.0	106.2
tHGp_e2_a12	–1292.72674	115.71	69.8	–91.1	–68.5	59.9	–151.2	–103.9
cHGp_e1_e33	–1292.72650	116.33	23.1	–160.5	–60.8	–149.2	170.1	–66.6
cHGp_e2_e33	–1292.72614	117.30	75.4	–162.9	–64.8	–151.4	–161.4	–72.0
tHGp_e1_e27	–1292.72587	118.00	32.9	–160.1	–65.3	–62.5	163.2	94.8
tHGp_e1_e16	–1292.72512	119.96	21.7	–124.2	–63.8	45.1	166.5	45.1
tHGp_e1_a25	–1292.72406	122.77	36.4	–87.1	–65.7	–54.8	162.1	–21.4
tHGp_e1_e25	–1292.72359	123.99	37.4	–161.1	–66.0	–59.3	162.0	–24.9
tHGp_e1_e33	–1292.71592	144.11	30.0	–165.4	–65.4	–155.0	164.2	–74.6

3.1.3. IMIDAZOLE-PROPIONIC ACID-LIKE MODES (I AND IP MODE)

For the naming of the *cis* and *trans* conformers in the I mode, the relative position of N_{am} and N_π was used. A valence angle N_π–Cu–N_{am}' of < 120° led to a *cis* position, whereas a value of > 140° led to a *trans* position. The classification showed that a new type of arrangement around copper(II) emerged, in which both oxygen atoms of the same carboxylate group, O^1 and O^2 bind to copper(II). Thus, a four–membered chelate ring is formed that is illustrated in Figure 5. Since the notation *cis* and *trans* becomes meaningless in these structures, they are denoted as "2" instead of "c" or "t". To label structure details, the position of N_{am} relative to the binding O^1 atom is determined by the torsion angle N_{am}–C^α–C–O^1 as either *syn*, denoted as "s", or *anti* position, denoted as "a". Specifically, if the value of the optimized angle is between –120° and 0° it is classified as *syn*, otherwise as *anti*. It was not possible to clearly determine the orientation of N_{am} in the *2* conformers, because both oxygen atoms bind to copper(II). In such cases, we introduced the letter "u" for undefined. The optimized conformations of the seven-membered chelate ring resulted in a torsion angle triplet with defined signs classified as *b1* to *b6* as shown in Table 7.

Table 7: Classification of the seven-membered chelate ring in the I mode.

	b1	b2	b3	b4	b5	b6	b7
C^α–C^β–C^γ–N_π	+	–	–	+	+	–	–
C–C^α–C^β–C^γ	–	+	+	–	+	–	+
O^1–C–C^α–C^β	–	–	+	+	–	+	–
Cu–O^1–C–C^α		< 90°					> 90°

It was observed that many optimized conformations led to a *b2* conformation, but had a completely different Cu–O^1–C–C^α torsion angle. So we introduced a *b7* conformation with values of this torsion > 90°, whereas values < 90° remained a *b2* conformation. Altogether 46 *cis*, 58 *trans* and 4 *2* IGp equilibrium structures were observed, which are listed with their characteristics in Table 8.

Table 8: List of the optimized IGp geometries with the related torsion angles, electronic energy as well as the relative electronic energy. The reference value is the electronic energy of tGGp_a19_e12 (–1292.77081 a.u.).

symbol	electronic energy [a.u.]	rel. energy [kJ mol^{-1}]	Cu–N$_\pi$–C$^\gamma$–C$^\beta$ [°]	N$_\pi$–C$^\gamma$–C$^\beta$–C$^\alpha$ [°]	C$^\gamma$–C$^\beta$–C$^\alpha$–C [°]	C$^\beta$–C$^\alpha$–C–O^1 [°]	C$^\alpha$–C–O^1–Cu [°]	N$_{am}$–C$^\alpha$–C–O^1 [°]	N$_{am}$–C$^\alpha$–C$^\beta$–C$^\gamma$ [°]	Cu–N$_{am}$'–C$^{\alpha'}$–C$^{\beta'}$ [°]	N$_{am}$'–C$^{\alpha'}$–C$^{\beta'}$–C$^{\gamma'}$ [°]	C$^{\alpha'}$–C$^{\beta'}$–C$^{\gamma'}$–C$^{\delta'}$ [°]
tIGp_sb6_a22	–1292.76514	14.89	8.4	–12.6	–64.5	101.6	–14.8	–22.4	59.3	–76.8	–52.3	–93.5
tIGp_sb6_e12	–1292.76424	17.27	6.4	–9.9	–64.5	101.2	–13.6	–22.9	59.3	–157.4	61.8	–108.6
tIGp_sb3_a23	–1292.76329	19.76	7.6	–67.2	56.3	39.1	–109.3	–82.2	179.8	–80.1	–53.4	–85.8
tIGp_sb6_e38	–1292.76301	20.50	5.9	–9.1	–65.0	101.4	–14.2	–22.7	58.9	–157.7	–155.5	121.4
tIGp_ab1_e12	–1292.76238	22.14	–11.7	67.8	–50.8	–51.0	120.8	–175.3	75.5	–155.6	60.2	–108.2
tIGp_sb6_a17	–1292.76178	23.71	13.6	–19.2	–59.6	102.8	–17.4	–20.8	63.9	–86.8	70.4	104.5
tIGp_ab2_e12	–1292.76065	26.68	2.5	–50.2	98.7	–69.6	1.1	168.1	–136.7	–156.4	60.5	–107.0
tIGp_sb6_a38	–1292.76058	26.88	5.2	–8.1	–65.6	101.3	–14.0	–23.0	58.3	–98.5	–155.5	134.7
tIGp_ab7_e12	–1292.76045	27.22	23.0	–63.2	62.9	–84.3	113.9	156.2	–173.1	–155.5	60.1	–108.1
tIGp_sb4_a22	–1292.76007	28.20	–22.7	59.1	–65.8	94.3	–111.5	–29.5	61.3	–80.4	–54.8	–91.3
tIGp_ab1_e38	–1292.75973	29.09	–13.1	68.0	–50.9	–50.9	120.9	–175.2	75.4	–154.2	–155.5	122.6
tIGp_sb3_a17	–1292.75945	29.84	15.4	–72.5	53.2	43.5	–108.7	–77.9	177.0	–88.4	69.9	98.1
tIGp_sb3_e12	–1292.75911	30.73	11.1	–66.6	49.1	51.9	–119.2	–68.9	173.5	–156.7	61.1	–109.4
tIGp_sb3_e38	–1292.75825	32.98	12.5	–64.8	51.2	47.9	–119.9	–72.8	175.2	–148.4	–154.6	122.9
tIGp_ab2_e38	–1292.75823	33.03	1.1	–52.0	99.3	–67.1	–0.2	170.2	–135.7	–156.1	–156.2	122.0
tIGp_ab7_e38	–1292.75799	33.66	21.8	–63.5	63.8	–83.9	112.6	156.5	–172.2	–154.9	–156.2	121.5
tIGp_sb4_e12	–1292.75703	36.19	–20.6	61.5	–67.8	91.2	–110.4	–32.7	59.6	–155.8	61.9	–108.6
tIGp_sb6_a27	–1292.75610	38.64	6.1	–9.0	–65.0	101.9	–15.2	–22.2	58.9	–91.3	–65.3	98.3
tIGp_ab1_a22_A	–1292.75597	38.97	–13.6	68.2	–50.9	–51.1	119.1	–175.5	75.5	–73.0	–49.9	–100.5
tIGp_sb4_e38	–1292.75593	39.08	–21.9	61.1	–64.7	92.5	–114.8	–31.0	62.4	–147.6	–153.8	123.1
tIGp_sb6_e27	–1292.75587	39.24	6.4	–9.6	–64.6	101.8	–15.1	–22.2	59.2	–152.2	–68.5	92.5
tIGp_ab1_a22_B	–1292.75578	39.46	–12.5	68.9	–54.2	–44.9	114.9	–168.8	69.4	–73.0	–50.2	–101.0
tIGp_sb4_a12	–1292.75535	40.60	–18.8	69.0	–69.6	80.4	–106.2	–43.4	57.2	–98.8	68.6	–100.2
tIGp_ab7_a22	–1292.75511	41.23	14.9	–62.1	74.6	–85.3	96.4	154.3	–161.6	–75.1	–50.8	–99.9
tIGp_sb3_a12	–1292.75509	41.28	15.6	–64.7	62.3	26.0	–107.1	–95.8	–174.1	–99.4	74.2	–99.3
tIGp_sb4_a17	–1292.75509	41.29	–20.3	58.9	–66.9	91.9	–108.7	–32.0	60.4	–91.8	66.6	106.0
tIGp_ab1_a27	–1292.75467	42.37	–13.5	68.2	–50.9	–50.8	121.3	–175.1	75.4	–100.1	–62.5	102.5
tIGp_sb6_e24	–1292.75437	43.18	6.2	–9.5	–64.6	102.0	–15.5	–22.1	59.3	–155.7	–63.4	–34.3
tIGp_sb6_e16	–1292.75404	44.05	5.6	–8.5	–65.7	101.2	–13.1	–23.1	58.2	–151.1	53.1	68.7
tIGp_ab1_e27	–1292.75370	44.94	–12.3	68.0	–50.7	–51.2	120.8	–175.5	75.6	–147.7	–63.9	102.1
tIGp_sb3_a27	–1292.75295	46.90	11.4	–65.0	50.4	49.0	–119.9	–71.7	174.5	–87.8	–59.9	96.1
tIGp_ab1_a18	–1292.75233	48.54	–12.3	67.2	–55.9	–41.0	113.7	–165.3	67.7	–88.2	65.3	111.3
tIGp_ab7_a17	–1292.75218	48.91	21.1	–64.6	67.5	–83.8	107.1	156.2	–168.7	–88.3	69.0	107.5
tIGp_sb3_e27	–1292.75214	49.04	12.3	–64.8	50.6	48.8	–120.3	–71.8	174.7	–143.5	–67.6	96.6
tIGp_ab2_a27	–1292.75201	49.36	1.2	–47.9	98.0	–71.0	1.4	166.8	–137.5	–100.1	–64.0	103.7
tIGp_ab1_e16	–1292.75191	49.62	–10.3	69.4	–53.3	–46.8	116.1	–170.7	70.5	–152.0	49.7	57.2

Table 8 (continued).

symbol	electronic energy [a.u.]	rel. energy [kJ mol⁻¹]	Cu–Nπ–Cγ–Cβ [°]	Nπ–Cγ–Cβ–Cα [°]	Cγ–Cβ–Cα–C [°]	Cβ–Cα–C–O¹ [°]	Cα–C–O¹–Cu [°]	Nam–Cα–C–O¹ [°]	Nam–Cα–Cβ–Cγ [°]	Cu–Nam'–Cα'–Cβ' [°]	Nam'–Cα'–Cβ'–Cγ' [°]	Cα'–Cβ'–Cγ'–Cδ' [°]
tIGp_ab1_e25	−1292.75164	50.35	−12.6	67.9	−50.8	−50.9	120.9	−175.2	75.5	−151.6	−63.7	−21.0
tIGp_ab2_e27	−1292.75163	50.38	2.0	−50.1	98.6	−69.8	1.7	167.9	−136.8	−147.8	−65.7	100.2
tIGp_ab7_a27	−1292.75139	50.99	23.4	−59.7	61.4	−88.5	115.9	152.4	−175.0	−103.6	−62.2	104.0
tIGp_ab7_e27	−1292.75133	51.17	22.8	−62.0	62.7	−85.7	114.0	154.9	−173.5	−145.5	−63.9	104.1
cIGp_sb6_e12	−1292.75125	51.35	15.1	−30.9	−47.4	97.5	−11.0	−23.8	74.5	−156.9	59.9	−106.9
tIGp_ab2_e16	−1292.75119	51.52	2.4	−50.9	98.8	−68.8	0.8	168.7	−136.4	−153.5	49.7	63.9
tIGp_sb4_a27	−1292.75081	52.51	−23.1	61.7	−64.3	91.6	−115.0	−31.8	62.7	−92.2	−63.1	93.9
tIGp_ab7_e16	−1292.75049	53.35	22.7	−63.6	63.5	−83.6	112.5	156.7	−172.5	−152.4	50.3	68.2
tIGp_ab1_a16	−1292.75032	53.82	−8.8	71.7	−53.6	−47.2	112.0	−171.1	70.1	−91.4	50.0	68.0
2IGp_ub1_e12	−1292.75019	54.15	−29.5	65.5	−53.7	−59.9	143.9	177.3	71.7	−146.0	65.8	−105.7
tIGp_ab2_e25	−1292.74977	55.26	1.0	−51.0	99.3	−68.1	−0.1	169.3	−135.9	−150.8	−64.6	−25.0
tIGp_ab2_a24	−1292.74947	56.03	0.0	−50.4	99.1	−68.0	−0.2	169.4	−136.1	−99.5	−63.7	−30.1
tIGp_ab7_e25	−1292.74939	56.24	22.5	−62.3	62.9	−85.3	113.7	155.3	−173.3	−150.2	−65.7	−12.3
2IGp_ub7_e12	−1292.74906	57.12	28.1	−61.5	49.9	−101.1	143.5	139.4	173.8	−145.7	62.4	−105.7
tIGp_sb6_e33	−1292.74898	57.33	5.0	−7.5	−66.3	101.6	−14.2	−22.7	57.7	−161.1	−150.0	−65.0
tIGp_ab7_e22	−1292.74868	58.11	21.3	−63.5	64.5	−83.7	111.2	156.5	−171.4	−152.6	−70.3	−96.3
cIGp_sb6_e38	−1292.74792	60.10	15.9	−32.2	−46.5	97.5	−11.8	−23.7	75.3	−161.4	−156.3	121.3
tIGp_sb6_a35	−1292.74790	60.17	4.2	−6.9	−66.4	102.1	−15.5	−22.1	57.6	−79.7	−167.9	−21.4
tIGp_ab1_e33_A	−1292.74666	63.42	−13.7	66.6	−54.4	−43.5	118.1	−168.9	73.2	−161.3	−150.9	−77.5
tIGp_ab1_e33_B	−1292.74662	63.53	−14.7	65.7	−57.8	−35.9	113.7	−160.5	66.0	−160.8	−150.6	−78.1
tIGp_ab2_e33	−1292.74554	66.35	1.4	−51.8	99.3	−67.6	0.2	169.7	−135.7	−162.0	−150.8	−71.7
cIGp_sb6_a38	−1292.74524	67.14	15.3	−30.9	−47.4	98.0	−12.0	−23.4	74.5	−93.0	−155.5	135.0
tIGp_ab7_e33	−1292.74520	67.26	22.1	−63.2	63.5	−83.8	112.3	156.5	−172.5	−160.5	−150.7	−74.6
tIGp_sb3_e33	−1292.74486	68.15	11.8	−66.1	51.4	47.8	−117.8	−73.1	175.5	−156.6	−149.4	−68.2
tIGp_sb3_a35	−1292.74404	70.30	11.1	−65.2	51.1	47.8	−118.4	−72.9	175.2	−81.6	−168.5	−13.5
cIGp_ab1_a23	−1292.74295	73.17	−1.3	77.1	−55.4	−48.1	100.1	−171.4	68.2	−75.1	−44.1	−67.9
tIGp_sb4_a35	−1292.74277	73.62	−21.8	63.8	−66.1	88.7	−112.2	−34.9	60.8	−86.2	−165.2	−23.4
tIGp_sb4_e33	−1292.74259	74.11	−21.3	61.2	−66.1	91.9	−112.5	−31.8	61.1	−155.1	−148.0	−67.3
cIGp_sb6_e27	−1292.74208	75.44	14.6	−30.1	−48.0	98.1	−12.0	−23.1	73.9	−161.2	−66.6	91.5
cIGp_sb6_a27	−1292.74180	76.19	13.3	−28.1	−49.3	99.0	−13.0	−22.4	72.9	−92.0	−61.4	98.8
cIGp_ab1_e12	−1292.74126	77.60	−8.0	77.5	−48.6	−56.8	112.9	−178.8	74.2	−155.2	56.9	−106.2
cIGp_ab1_a12	−1292.74116	77.85	−3.6	84.1	−50.4	−48.5	79.3	−171.5	72.8	−87.7	38.0	−115.8
cIGp_ab5_a12	−1292.74084	78.70	−21.9	34.0	46.6	−90.4	5.1	148.4	171.2	−88.6	42.0	−118.7
2IGp_ub1_e16	−1292.74052	79.53	−34.2	68.9	−53.4	−61.7	143.7	175.7	71.9	−146.2	56.0	70.6
cIGp_ab5_e12	−1292.74015	80.51	−21.3	30.5	49.5	−91.3	4.4	147.8	173.9	−155.9	58.2	−107.3

Table 8 (continued).

symbol	electronic energy [a.u.]	rel. energy [kJ mol⁻¹]	Cu–Nπ–Cγ–Cβ [°]	Nπ–Cγ–Cβ–Cα [°]	Cγ–Cβ–Cα–C [°]	Cβ–Cα–C–O¹ [°]	Cα–C–O¹–Cu [°]	Nam–Cα–C–O¹ [°]	Nam–Cα–Cβ–Cγ [°]	Cu–Nam'–Cα'–Cβ' [°]	Nam'–Cα'–Cβ'–Cγ' [°]	Cα'–Cβ'–Cγ'–Cδ' [°]
clGp_sb6_e24	–1292.74014	80.53	14.9	–30.4	–47.8	98.3	–12.3	–23.0	74.2	–162.0	–60.1	–31.2
clGp_ab7_a23	–1292.73975	81.55	30.2	–62.2	55.4	–93.8	128.4	147.5	179.3	–80.2	–46.3	–82.1
clGp_sb6_e16	–1292.73861	84.55	16.1	–32.4	–46.4	97.5	–11.4	–23.6	75.4	–154.5	48.5	52.8
clGp_sb6_a25	–1292.73820	85.64	13.6	–28.8	–48.7	99.2	–13.5	–22.2	73.4	–93.7	–60.3	–22.0
clGp_ab1_e38	–1292.73690	89.05	–6.0	76.2	–49.4	–56.3	115.0	–178.2	73.2	–160.7	–156.3	121.5
2lGp_ub7_e16	–1292.73690	89.05	26.4	–58.4	49.5	–101.0	139.2	139.9	173.3	–144.6	52.1	66.8
clGp_ab5_e38	–1292.73616	90.97	–20.4	31.7	47.9	–89.5	4.0	149.8	172.2	–159.6	–155.1	121.6
clGp_ab7_a12	–1292.73518	93.54	23.2	–68.5	66.7	–82.1	116.2	158.6	–169.6	–101.0	35.6	–117.7
clGp_ab1_a38	–1292.73451	95.32	–4.5	87.9	–49.1	–41.1	47.8	–164.3	74.0	–89.6	–157.0	135.2
clGp_ab5_a38	–1292.73440	95.59	–20.6	32.1	48.0	–89.4	3.3	149.8	172.3	–90.9	–157.3	135.4
clGp_ab7_a27	–1292.73304	99.19	29.0	–62.8	53.4	–94.1	131.7	147.6	176.9	–83.1	–58.4	97.5
clGp_ab5_a27	–1292.73291	99.52	–20.5	29.6	50.2	–90.5	4.1	148.8	174.3	–87.5	–55.8	99.4
clGp_sb3_a12	–1292.73282	99.75	4.1	–72.2	46.1	59.7	–115.5	–60.8	171.1	–92.0	48.4	–121.0
clGp_ab1_a27	–1292.73275	99.94	–4.6	87.7	–49.7	–41.5	51.7	–164.9	73.6	–88.4	–58.3	98.5
clGp_sb6_e33	–1292.73195	102.03	16.5	–32.8	–46.2	97.6	–11.7	–23.4	75.6	–163.9	–151.8	–63.8
clGp_sb3_a38	–1292.73172	102.64	4.5	–72.5	45.6	60.5	–115.9	–59.7	170.5	–87.7	–157.5	135.5
clGp_ab1_e27	–1292.73151	103.19	–5.8	75.0	–49.7	–56.1	117.0	–178.1	73.2	–158.3	–63.1	95.1
clGp_ab5_e27	–1292.73100	104.54	–20.0	29.5	49.9	–90.3	4.2	149.1	174.0	–157.7	–63.8	93.1
clGp_sb3_a28	–1292.73097	104.61	13.5	–61.5	46.6	59.5	–133.8	–59.6	170.9	–96.6	–55.3	110.6
clGp_ab5_a24	–1292.73062	105.54	–19.3	28.1	50.9	–90.5	4.7	149.0	174.9	–82.1	–52.7	–35.3
clGp_sb3_a27	–1292.73016	106.74	0.7	–82.3	47.0	44.8	–52.9	–78.5	172.3	–91.5	–57.9	98.2
clGp_sb3_e27	–1292.72972	107.88	12.3	–61.6	46.8	59.4	–133.2	–59.8	171.1	–165.3	–60.4	100.3
clGp_ab1_e25	–1292.72959	108.22	–4.8	74.6	–49.8	–55.9	116.8	–178.0	73.0	–159.8	–59.6	–25.9
clGp_ab5_e25	–1292.72916	109.36	–19.2	28.9	50.1	–90.4	4.6	149.0	174.1	–160.3	–59.1	–27.5
clGp_ab1_e16_A	–1292.72888	110.11	–10.5	79.9	–48.0	–57.4	109.0	–179.6	74.9	–130.4	44.8	43.3
clGp_ab1_a18	–1292.72825	111.76	–7.8	66.8	–51.6	–54.8	127.1	–177.8	72.9	–100.8	84.9	120.5
clGp_ab5_a16	–1292.72806	112.25	–23.5	32.0	49.2	–93.1	6.2	145.7	173.7	–115.2	44.0	48.1
clGp_ab5_e16	–1292.72741	113.96	–21.5	31.3	49.0	–91.2	4.0	148.0	173.4	–152.3	46.0	40.4
clGp_sb3_e25	–1292.72715	114.63	13.2	–61.8	46.8	59.8	–133.7	–59.4	171.1	–166.3	–59.7	–22.8
clGp_ab1_e16_B	–1292.72688	115.35	–4.2	87.6	–48.4	–42.4	49.3	–165.5	74.6	–153.8	47.3	39.5
clGp_sb3_a25	–1292.72662	116.03	5.0	–71.7	45.8	60.2	–117.9	–60.0	170.6	–88.3	–57.6	–27.9
clGp_sb3_a16	–1292.72346	124.33	3.5	–73.3	45.3	61.1	–112.7	–59.3	170.4	–92.6	47.7	54.4
clGp_ab1_a35	–1292.72166	129.06	–4.0	87.9	–50.8	–40.3	49.7	–164.0	72.7	–76.3	–169.8	–0.7
clGp_ab1_e33	–1292.72143	129.67	–6.2	77.4	–49.4	–56.5	112.9	–178.4	73.2	–166.1	–152.2	–67.5
clGp_ab5_e33	–1292.72087	131.13	–21.6	33.7	46.7	–89.5	3.9	149.8	171.0	–164.8	–151.1	–65.8
clGp_ab5_a17	–1292.71891	136.28	–19.7	32.2	46.8	–90.3	6.3	149.4	170.6	–92.4	70.4	99.6
clGp_sb3_a35	–1292.71753	139.90	6.6	–73.2	44.7	61.8	–116.1	–58.4	169.6	–79.2	–164.4	–19.4

For the Ip mode, the optimization gave completely different results. Nearly all initial structures ended up with a coordination number of less than four (Figure 6). These conformers were not analyzed further because structures with less than four atoms binding to copper were not outlined as physiologically important species in experimental studies [12]. Just 33 structures in this mode remained stable by forming bonds to both carboxylate oxygen atoms O^1 and O^2, and are denoted as *2* at the beginning of the symbol like in the I mode. The torsion angle $C–C^\alpha–C^\beta–C^\gamma$ in these *2* conformers can be either negative, labelled with "m" or positive, labelled with "p". This is followed by one digit for one of eight possible ranges for the angle $C^\alpha–C^\beta–C^\gamma–C^\delta$: > 130° *(1),* 120° to 130° *(2),* 110° to 120° *(3),* 100° to 110° *(4),* 0° to 100° *(5),* −100° to 0° *(6),* −110° to −100° *(7)* and < −110° *(8).* The stable IpGp equilibrium structures with their characteristic data are listed in Table 9.

cIpGp_m1_a12   tIpGp_p4_e25
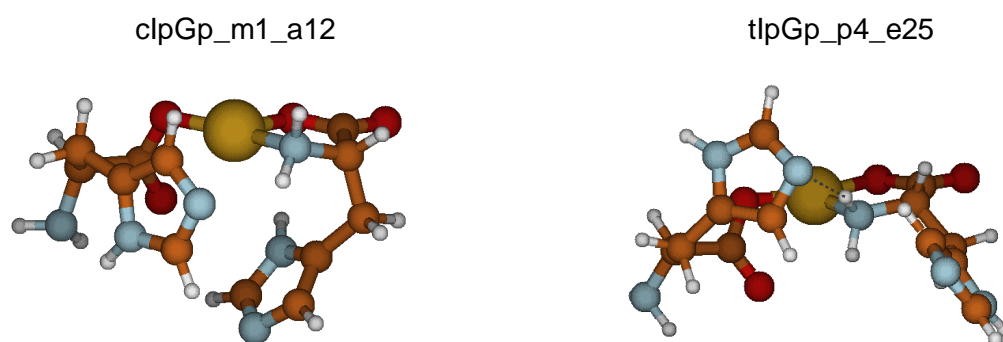
Figure 6: Examples for equilibrium structures in the Ip mode with less than four binding atoms to copper(II).

Table 9: List of the optimized lpGp geometries with the related torsion angles, electronic energy as well as the relative electronic energy. The reference value is the electronic energy of tGGp_a19_e12 (–1292.77081 a.u.).

symbol	electronic energy [a.u.]	rel. energy [kJ mol⁻¹]	N_T–C^δ–C^γ–C^β [°]	C^δ–C^γ–C^β–C^α [°]	C^γ–C^β–C^α–C [°]	C^β–C^α–C–O^1 [°]	C^α–C–O^1–Cu [°]	Cu–N_{am}'–$C^{\alpha'}$–$C^{\beta'}$ [°]	N_{am}'–$C^{\alpha'}$–$C^{\beta'}$–$C^{\gamma'}$ [°]	$C^{\alpha'}$–$C^{\beta'}$–$C^{\gamma'}$–$C^{\delta'}$ [°]
2lpGp_m2_a24	–1292.75013	54.30	–173.6	120.0	–51.0	–47.8	166.4	–88.4	–59.5	–52.6
2lpGp_m6_e12	–1292.74766	60.79	–179.3	–99.9	–64.1	157.8	177.6	–153.2	59.1	–106.0
2lpGp_m1_e12	–1292.74745	61.35	178.1	134.7	–59.9	–46.5	–179.1	–156.2	59.1	–108.1
2lpGp_p6_a23	–1292.74520	67.25	172.7	–96.8	48.7	–97.5	167.1	–91.2	–59.5	–67.0
2lpGp_m1_e38	–1292.74502	67.72	179.1	133.4	–58.3	–45.4	178.6	–154.9	–154.9	120.8
2lpGp_m2_e12	–1292.74478	68.36	–171.1	121.5	–46.9	–39.4	159.8	–142.4	64.7	–104.9
2lpGp_m6_e38	–1292.74398	70.46	–179.3	–99.7	–64.0	157.5	178.1	–156.0	–155.1	120.9
2lpGp_m3_e38	–1292.74385	70.81	–168.9	118.2	–45.0	–47.1	156.2	–151.2	–153.9	122.1
2lpGp_p8_e12	–1292.74347	71.80	179.5	–113.5	50.8	64.8	–177.1	–154.6	59.1	–106.7
2lpGp_p6_e38	–1292.74326	72.35	170.0	–93.6	42.0	–92.8	156.0	–150.0	–153.9	122.2
2lpGp_m1_a38	–1292.74251	74.31	179.0	133.2	–58.1	–47.3	178.5	–99.6	–155.0	132.5
2lpGp_p6_e12	–1292.74232	74.81	169.9	–92.0	41.0	–93.6	156.6	–159.6	61.4	–113.8
2lpGp_m4_a27	–1292.74075	78.94	–168.8	104.3	–50.9	103.6	–153.7	–102.1	–60.2	102.3
2lpGp_m2_a27	–1292.74053	79.50	–176.5	126.2	–52.5	–45.9	169.3	–95.0	–58.0	105.5
2lpGp_m6_a27	–1292.74001	80.88	–179.3	–99.9	–63.4	155.7	178.4	–96.8	–59.9	99.3
2lpGp_p8_e38	–1292.73967	81.76	179.6	–113.8	50.6	64.8	–177.4	–155.5	–155.8	121.4
2lpGp_p7_e28	–1292.73927	82.81	177.0	–108.7	37.7	65.7	–161.9	–174.6	–58.4	132.7
2lpGp_m3_e27	–1292.73889	83.82	–169.6	119.8	–46.2	–46.3	156.3	–143.6	–63.9	93.1
2lpGp_m2_e17	–1292.73854	84.74	–170.1	122.8	–47.8	–43.5	159.0	–146.4	65.8	100.7
2lpGp_p6_e27	–1292.73828	85.41	170.1	–94.5	41.9	–92.4	157.2	–140.0	–63.2	95.4
2lpGp_p6_e17	–1292.73796	86.25	171.8	–96.6	44.1	–90.7	160.2	–132.4	69.6	100.9
2lpGp_m4_a25	–1292.73780	86.69	–168.7	103.7	–51.1	103.7	–153.4	–103.9	–60.7	–20.0
2lpGp_p6_a38	–1292.73779	86.72	170.6	–97.8	23.6	72.3	–159.0	–100.8	–154.9	132.8
2lpGp_m7_a27	–1292.73749	87.49	–178.8	–103.1	–66.0	–22.2	–174.9	–96.1	–59.0	99.8
2lpGp_m7_e16	–1292.73704	88.68	–179.2	–100.7	–64.6	159.6	177.7	–151.3	48.2	48.9
2lpGp_p7_a27	–1292.73518	93.56	171.3	–100.9	24.0	72.2	–158.8	–98.9	–61.0	101.2
2lpGp_p8_e16	–1292.73240	100.86	–179.9	–118.3	50.1	66.1	–177.5	–153.0	47.4	52.0
2lpGp_p7_e24	–1292.73206	101.75	174.7	–105.7	32.5	70.3	–159.6	–165.0	–62.8	–30.1
2lpGp_p8_e31	–1292.73099	104.56	177.4	–114.4	35.9	69.8	–161.0	–177.0	–147.7	–137.1
2lpGp_p6_a22	–1292.73088	104.84	172.3	–98.8	27.2	–98.5	156.7	–76.6	–46.4	–94.7
2lpGp_m3_e33	–1292.73051	105.83	–169.4	119.6	–45.8	–45.8	156.6	–153.1	–146.4	–60.5
2lpGp_p6_e33	–1292.72923	109.17	170.2	–94.3	42.6	–92.9	156.4	–153.3	–147.2	–61.9
2lpGp_p7_a17	–1292.72836	111.47	171.4	–100.1	23.2	74.4	–158.6	–90.2	64.3	103.8

3.2. CONFORMATIONAL ANALYSIS

3.2.1. ENERGY LANDSCAPES

To get an overview of the conformer stability in the different coordination modes, the relative electronic energy values are plotted in Figure 7 with the reference value of –1292.77081 a.u. of the most stable conformer tGGp_a19_e12.
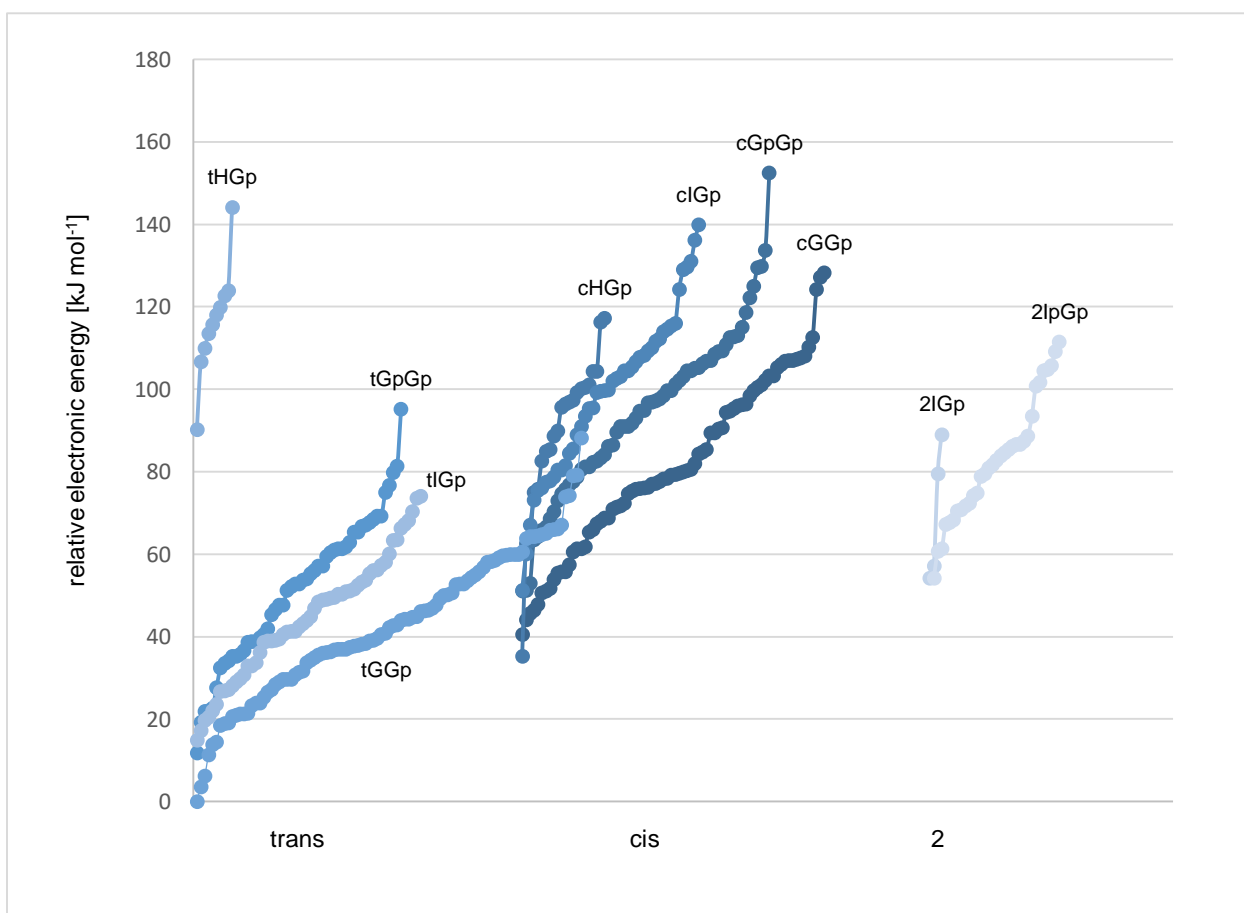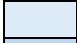

Figure 7: Relative B3LYP electronic energy values for the conformers of Cu(L-His)$_2$.
The reference value is the electronic energy of tGGp_a19_e12 (–1292.77081 a.u.).

As in previous work [12], the *trans* configuration is more stable than the *cis* one for the GGp, GpGp and IGp mode, whereas the reverse stability is obtained for the HGp conformers. The *2* conformers in the IGp mode are energetically between the *cis* and *trans* configurations, while in the IpGp mode these are the only stable ones. In general, the most stable equilibrium structures were found in the *trans* GGp coordination mode, the least stable ones in the HGp coordination mode, also in *trans* configuration. The Cu(L-His)$_2$ conformer of highest relative electronic energy (152.5 kJ mol^{-1}) is cGpGp_e33_e33.

3.2.2. DISTRIBUTION OF THE OPTIMIZED CONFORMERS

To compare the optimized equilibrium structures with respect to appearance and relative energy for each coordination mode, grid figures were constructed (Figure 9 – Figure 13). The field marked in yellow in Figure 11 indicates the global minimum structure tGGp_a19_e12, to which all other electronic energies refer. The energies were color-coded as shown in Table 10.

Table 10: Sectors for the relative B3LYP electronic energies with their associated color.

	kJ mol^{-1}
	0.0
	0.1 – 20.0
	20.1 – 40.0
	40.1 – 60.0
	60.1 – 80.0
	80.1 – 100.0
	100.1 – 120.0
	> 120.0

These grid figures do not merely mirror the already known behavior in relative B3LYP electronic energy, they also show the distribution of the optimized conformers.

As already noticed in Figure 7, the *trans* conformers have a higher relative electronic energy only in the HGp mode, whereas in all other modes this is the more stable configuration. It can also be seen that in the HGp mode more *cis* structures remained stable during the geometry optimization (Figure 9). Nearly all *trans* structures are present in the *cis* configuration too, with two exceptions: e1_a25 and e1_e25. It is evident that in the H mode the *e2* conformation is more stable than *e1* only for the *cis* conformers, which is also indicated in Figure 9. Generally, the equatorial position of the carboxylate group in the H mode is more preferred. In contrast, in the GGp coordination mode more *trans* conformers remained stable during the optimization with significantly lower electronic energies (Figure 11). The GGp conformer distribution of *cis* and *trans* is very similar, with two noticeable differences: the *a18* conformation occurs only in *cis* conformers, whereas *a36* occurs only in *trans* conformers. In general, the axial position of the C^β is slightly preferred in the G mode as well as in the Gp mode.

For conformers that ended in an equatorial-axial (*e-a*) combination in the GpGp coordination mode, the two L-His residues were interchanged to *a-e* in order to achieve a consistent nomenclature (Figure 12). As in the GGp mode, the *trans* conformers show a significantly lower B3LYP electronic energy, while the conformer distribution is very similar in both.

In the IGp coordination mode however, the decisive position of the N_{am} atom is clearly defined as equatorial or axial in the *trans* and *cis* conformers, whereas in the *2* conformers only "undefined" positions were spotted, which is due to the other binding oxygen O^2 (Figure 5). Much more *trans* than *cis* IGp conformations are stable with noticeably lower electronic energies. The conformer distribution differs from *cis* to *trans* configuration much more than in the other coordination modes (Figure 13). By shifting the proton from N_τ to N_π in the Ip mode, the *cis* conformation was converted almost completely to the *2* conformation, which is seen in Figure 10, only two of the initial structures ended up with less than four coordinating atoms like all *trans* conformers. One conformation, 2IpGp_m2_a24 is noticeable more stable than all other IpGp ones due to the presence of a hydrogen bond, which is depicted in Figure 8. Also evident is the preferred equatorial position of the C^β in the second Gp part in combination with this *2* configuration.
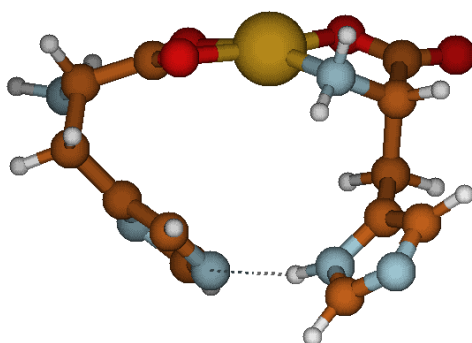
Figure 8: The most stable equilibrium structure in the IpGp mode.
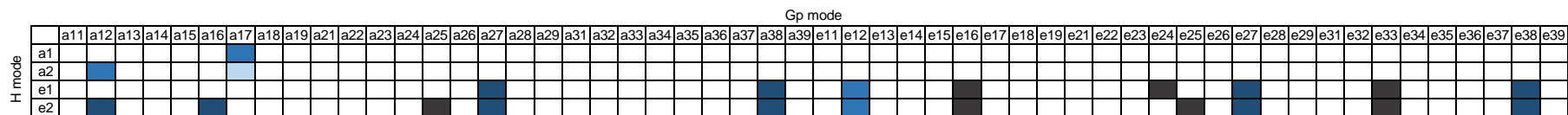
tHGp
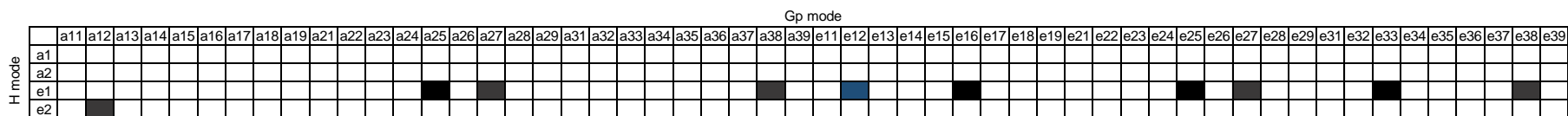
cHGp

Figure 9: Distribution of trans and cis Cu(L-His)₂ conformers with respect to structure and energy in the HGp mode.
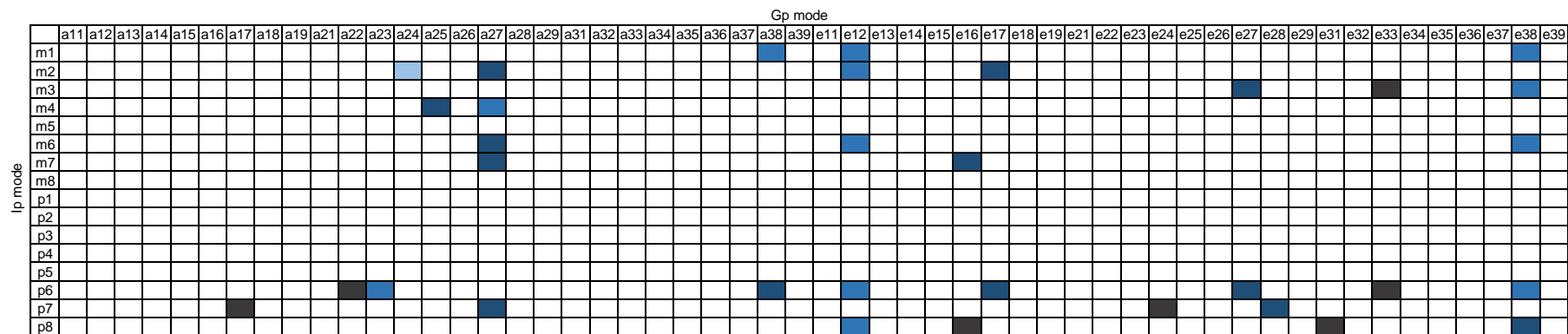
2lpGp

Figure 10: Distribution of 2 Cu(L-His)₂ conformers with respect to structure and energy in the IpGp mode.

tGGp

Figure 11: Distribution of trans and cis Cu(L-His)₂ conformers with respect to structure and energy in the GGp mode.

cGGp

Figure 11 (continued).

tGpGp

Figure 12: Distribution of trans and cis Cu(L-His)₂ conformers with respect to structure and energy in the GpGp mode.

cGpGp

Figure 12 (continued).

tIGp

cIGp

Figure 13: Distribution of trans, cis and 2 Cu(L-His)₂ conformers with respect to structure and energy in the IGp mode.

2IGp

Gp mode

I mode

a11 a12 a13 a14 a15 a16 a17 a18 a19 a21 a22 a23 a24 a25 a26 a27 a28 a29 a31 a32 a33 a34 a35 a36 a37 a38 a39 e11 e12 e13 e14 e15 e16 e17 e18 e19 e21 e22 e23 e24 e25 e26 e27 e28 e29 e31 e32 e33 e34 e35 e36 e37 e38 e39

ab1 ab2 ab3 ab4 ab5 ab6 ab7 sb1 sb2 sb3 sb4 sb5 sb6 sb7 ub1 ub2 ub3 ub4 ub5 ub6 ub7

Figure 13 (continued).

3.2.3. HYDROGEN BONDS

Due to the positive stabilization effects of hydrogen bonds in complexes in general, analyses of existing *intra-* as well as *inter*-residual hydrogen bonds within the conformers were performed. The number of hydrogen bonds present in each mode is listed in Table 11.

In general, the highest number of hydrogen bonds is formed in the GGp mode with a total of 71 in the *cis* conformers and 96 in the *trans* ones. These high numbers also explain the pronounced stability of this mode, especially for the *trans* conformation. The most hydrogen bonds present in this mode are *intra*-residual, $N_{am}–H_{am}\cdots N_{\pi}$ in the first L-His residue and $N_{\pi}'–H_p'\cdots O^{1'}$ in the other. The H-bond $N_{\pi}'–H_p'\cdots O^{1'}$ is the only one that is formed in each coordination mode at least once (Figure 14). In comparison to that, the next highest number, a total of 101 hydrogen bonds, is detected in the GpGp mode, which also matches with the second highest stability of these conformers. Although *inter*-residual hydrogen bonds are present in 4 of 10 conformers having the lowest electronic energy for the corresponding mode (Figure 5), such bonds are generally less common in all coordination modes due to the larger distances between the atoms.

tGGp_a37_a12   cGpGp_a12_a38
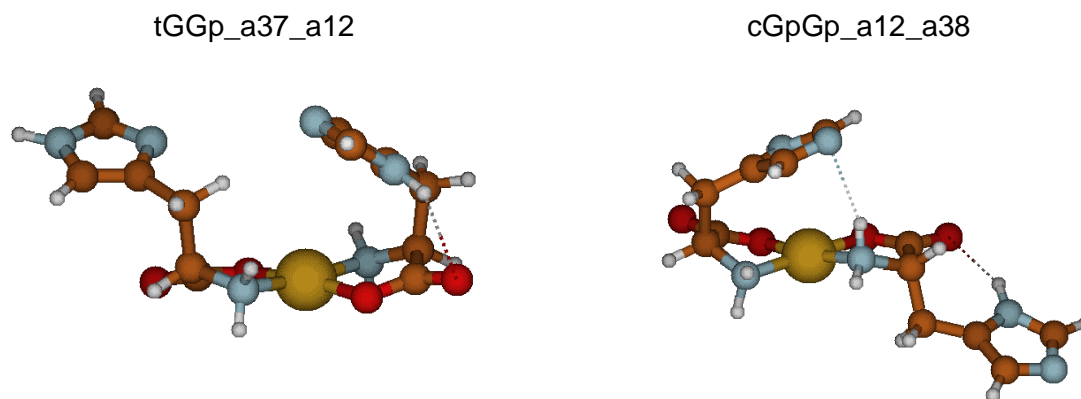
Figure 14: Examples of Cu(L-His)$_2$ conformers with the most common intra-residual hydrogen bond $N_{\pi}'–H_p'\cdots O^{1'}$ (dashed line) in the right L-His residue (Gp mode).

Table 11: Number and type of intra- and inter-residual D–H⋯A bonds shorter than 2.6 Å with an angle criterion of D–H⋯A > 110° in the B3LYP-optimized geometries of the trans and cis Cu(L-His)$_2$ conformers in different coordination modes.

D–H⋯A	GGp		GpGp		HGp			IGp		lpGp
	cis	trans	cis	trans	cis	trans	2	cis	trans	2
intra										
N_{am}–H_{am}⋯N_τ										
N_{am}–H_{am}⋯N_π	34	38		1						
N_τ–H_p⋯O^1										
N_π–H_p⋯O^1			15	17						4
N_τ–H_p⋯O^2										
N_π–H_p⋯O^2										1
N_τ–H_p⋯N_{am}										
N_π–H_p⋯N_{am}										12
N_{am}'–H_{am}'⋯N_τ'										
N_{am}'–H_{am}'⋯N_π'		6							6	1
N_π'–H_p'⋯$O^{1'}$	21	35	22	17	7	3	2	10	15	12
N_π'–H_p'⋯$O^{2'}$	5							3		
N_π'– H_p'⋯N_{am}'										
inter										
N_τ–H_p⋯$O^{1'}$	2									
N_π–H_p⋯$O^{1'}$										
N_τ–H_p⋯$O^{2'}$										
N_π–H_p⋯$O^{2'}$				1						
N_τ–H_p⋯N_{am}'										
N_π–H_p⋯N_{am}'										
N_τ–H_p⋯N_τ'		4								
N_π–H_p⋯N_τ'										
N_τ–H_p⋯N_π'										
N_π–H_p⋯N_π'										
N_{am}–H_{am}⋯N_τ'	6	4	3							
N_{am}–H_{am}⋯N_π'										
N_π'–H_p'⋯O^1								4	4	1
N_π'–H_p'⋯O^2		7			1				7	
N_π'–H_p'⋯N_{am}										
N_π'–H_p'⋯N_τ			1	3						6
N_π'–H_p'⋯N_π		2								
N_{am}'–H_{am}'⋯N_τ			12	9						15
N_{am}'–H_{am}'⋯N_π	3									

3.2.4. APICAL CU–DONOR DISTANCES

In low molecular weight copper(II) coordination compounds typically four nearby donor atoms arrange approximately in a plane around the metal ion, with the possibility of one or two more donor atoms, which are placed axially above or below this plane. These *apical* atoms are usually more distant due to the Jahn-Teller effect [33] [34] [35].

Figure 15 shows two examples of these possible axial donor atoms N_π and N_τ in the GGp mode, N_τ in the GpGp mode, O^1, O^2 and N_τ in the HGp mode and N_{am} and N_τ in the IGp and IpGp mode. The number and values of apical Cu–donor distances formed are listed in Table 12 for each coordination mode.

cGGp_a18_e38

Cu–N_π (2.37 Å)

tIGp_ab6_a17

Cu–N_{am} (2.33 Å)
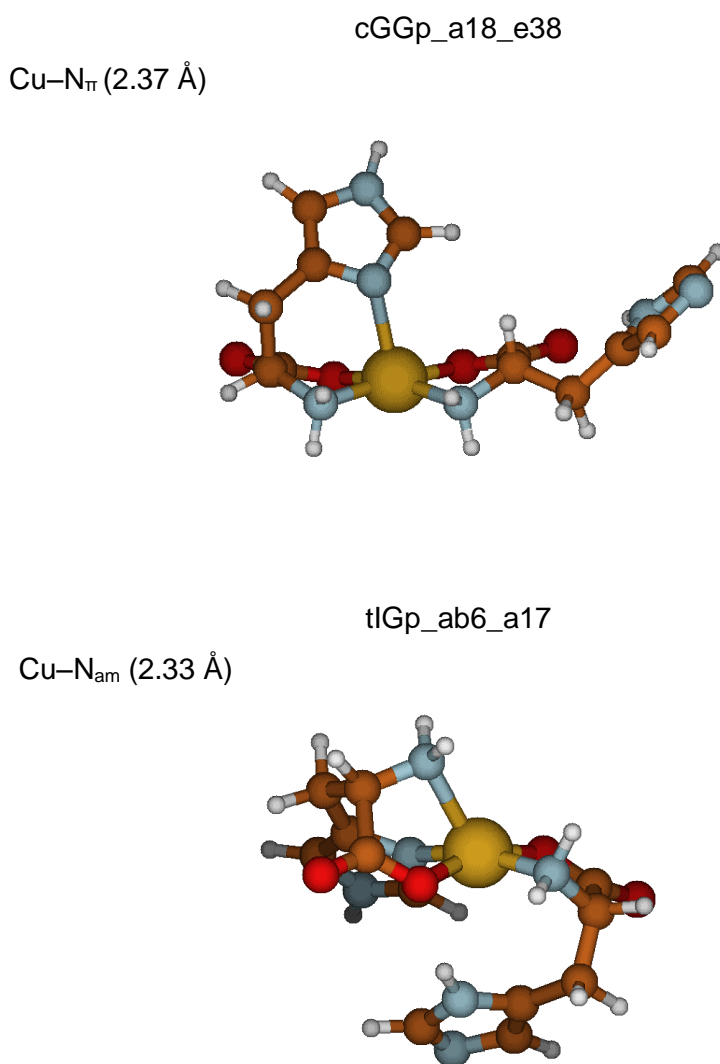
Figure 15: Examples of the Cu(L-His)₂ conformers with the type and value (in parentheses) of formed apical Cu–donor distances.

Table 12: Means and standard deviations (in parentheses) of the Cu–donor apical bond distances (<2.6 Å) in a number (n) of cis and trans Cu(L-His)$_2$ conformers.

	Cu–N$_\pi$ [Å]	n	Cu–N$_\tau$ [Å]	n	Cu–N$_{am}$ [Å]	n	Cu–O^1 [Å]	n	Cu–O^2 [Å]	n
cis										
GGp	2.38 (±0.02)	11								
GpGp										
HGp										
IGp					2.29 (±0.01)	9				
trans										
GGp	2.39 (±0.02)	8								
GpGp										
HGp										
IGp					2.35 (±0.01)	11				
2										
IGp	2.51 (±0.08)	4								
IpGp										

Table 13: Means and standard deviations (in parentheses) of the distances between copper(II) and N$_\pi$ (<3.0 Å) to point out the interaction with the imidazole ring in a number (n) of cis and trans Cu(L-His)$_2$ conformers.

	Cu–N$_\pi$ [Å]	n
cis		
GGp	2.93 (±0.03)	3
GpGp	2.98 (±0.01)	3
HGp		
IGp	2.86 (±0.03)	2
trans		
GGp		
GpGp		
HGp		
IGp	2.97	1
2		
IGp		
IpGp		

In the GpGp, HGp and IpGp mode, no apical bonds were detected at all, whereas an interaction of Cu with the imidazole ring was found in the GpGp mode as well as in the GGp and IGp mode (Table 13). Examples of Cu(L-His)$_2$ conformers with such an interaction are depicted in Figure 16. Such an interaction with the whole conjugated system may stabilize the complex the same way as a hydrogen bond. However, most apical bonds are formed in *cis* GGp and *trans* IGp conformers. In all cases, only the L-His part in G or I mode forms an apical bond between the unprotonated N_π (G mode) or the N_{am} (I mode) and copper(II). The absence of an apical bond between copper(II) and N_τ in the Gp mode can be explained by the larger chain length between these two atoms and the steric hindrance of the C^δ–H group. No intramolecular apical Cu–O is present in any of the 466 equilibrium structures (Table 12).

cGpGp_a12_a25

Cu–N_π distance: 2.97 Å
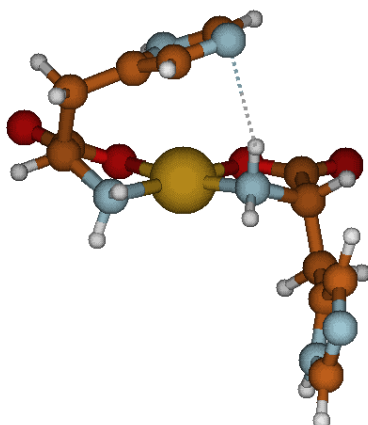
cIGp_ab1_a12

Cu–N_π distance: 2.83 Å
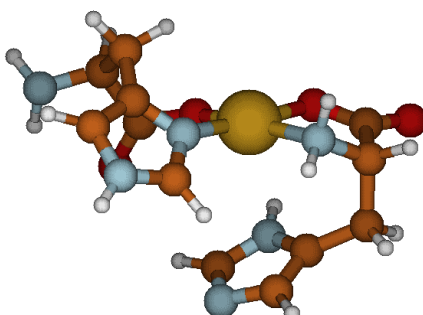
Figure 16: Examples of Cu(L-His)$_2$ conformers with an interaction between copper and the imidazole ring.

3.2.5. COPPER(II) COORDINATION POLYHEDRON

To examine the arrangement of the four nearby donor atoms around copper(II), the position of the binding atoms of the L-His residues relative to each other was analyzed. The perfect in-plane coordination is observed when the torsion angle connecting these atoms is 0° in the *cis* and ±180° in the *trans* configuration. The more the angle deviates from these values, the more distorted the coordination is. The following torsion angles were chosen to describe the distortion from planar copper(II) coordination geometry of the *trans* and *cis* conformers: $O^1–N_{am}–N_{am}'–O^{1''}$ for the GGp and GpGp mode, $N_π–N_{am}–N_{am}'–O^{1''}$ for the HGp mode and $N_π–O^1–N_{am}'–O^{1''}$ for the IGp mode. The *2* configuration in the IGp and lpGp mode was described with the torsion angle $O^1–O^2–N_{am}'–O^{1''}$. The correlation between distortion and relative energy is illustrated in Figure 17.
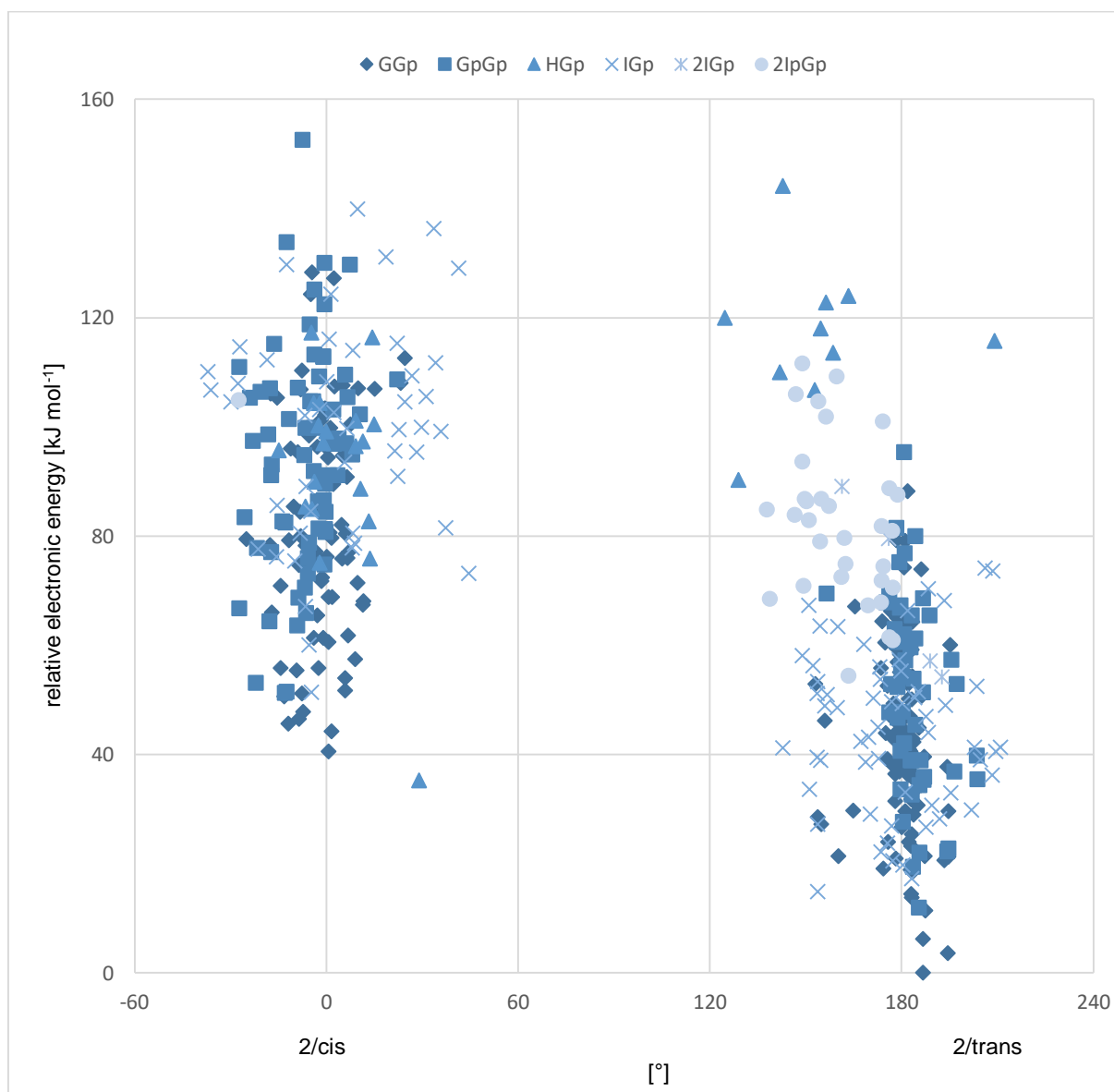
Figure 17: Correlation between the plane distortion around copper(II) and the relative energy (reference: tGGp_a19_e12) of the trans, cis and 2 Cu(L-His)₂ conformers in the GGp, GpGp, HGp, IGp and lpGp mode.

Most torsion angle values of the Cu(L-His)$_2$ conformers are near the planar coordination with values around 0° and 180°. It can also be noticed that for nearly all conformers the approximate square-planar arrangement becomes more distorted at higher energy values, except of the *cis* configuration in the IGp mode, which shows a more flexible distribution. Figure 18 depicts the extremes: the conformation with the highest distortion of the plane and the conformation with the most ideal in-plane coordination, both in the HGp mode. The highly distorted coordination around copper(II) in the tHGp_e1_e16 conformer shows already a tendency towards a distorted tetrahedral coordination.

tHGp_e1_e16

N_{π}–N_{am}–N_{am}'–$O^{1'}$: 124.7°

cHGp_e2_e27

N_{π}–N_{am}–N_{am}'–$O^{1'}$: 0.1°
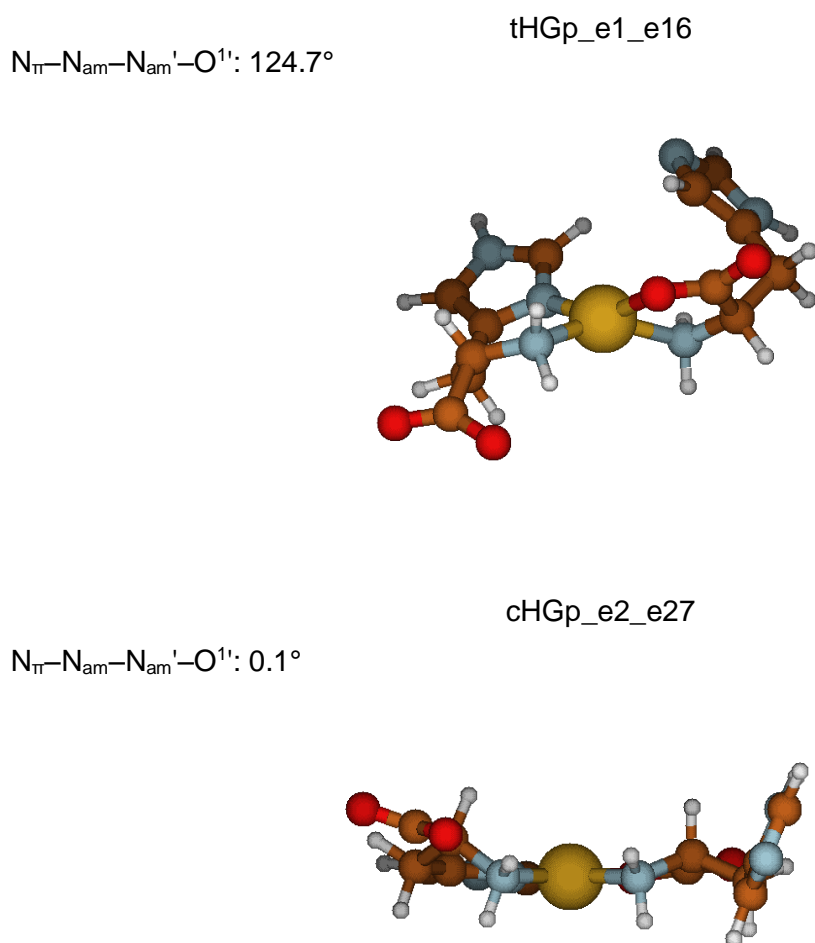
Figure 18: The most distorted (tetrahedral) and in-plane coordination around copper(II) of Cu(L-His)$_2$ equilibrium conformers in the HGp mode.

Yet another coordination type around copper(II) is found in the *2* configuration in the IGp and IpGp mode. The L-His residue with the two binding oxygen atoms O^1 and O^2 is always in-plane with the copper(II) atom. If a third binding atom of the other L-His residue is also in-plane and

the fourth one out of plane, a distorted trigonal pyramidal coordination is obtained as illustrated in Figure 19.
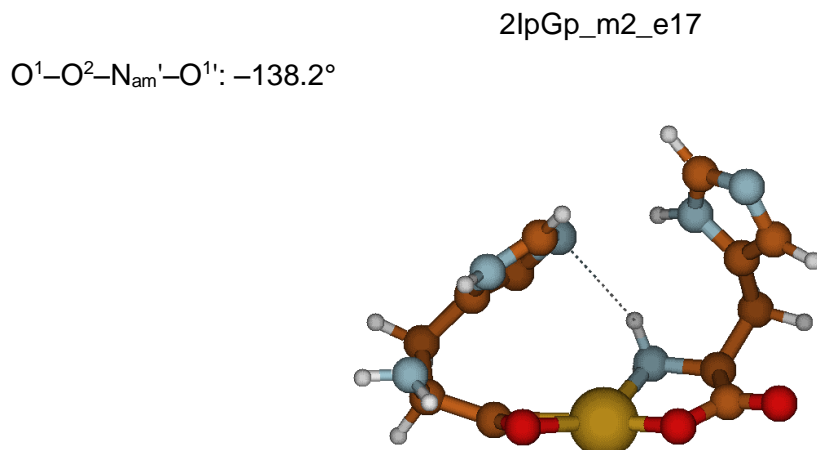
2lpGp_m2_e17

O^1–O^2–N_{am}'–$O^{1''}$: –138.2°

Figure 19: Example of a 2 Cu(L-His)$_2$ conformer with a trigonal pyramidal coordination around copper(II) in the lpGp mode.

In addition to the torsion angle analysis, the in-plane bond lengths Cu–O^1, Cu–O^2, Cu–N_{am} and Cu–N_{π} and six valence angles around the copper(II) atom were analyzed (Table 14). The values of the angles around copper(II) should be around 180° if the respective atoms are in *trans* position and about 90° when they are in *cis* position. According to the calculated mean and standard-deviation values, nearly all Cu(L-His)$_2$ conformers have an in-plane or distorted planar geometry that is in agreement with the torsion angle analysis. Again, in the HGp, IGp and lpGp modes high standard deviations and varying values are detected, which indicate the highest distortion from the square-planar to the distorted tetrahedral and trigonal pyramidal coordination geometry. These results are in agreement with previous studies [36], in which the planar coordination geometry is an electronically favored structure for Cu(aa)$_2$ complexes. The strain in the chelate rings due to crystal lattice effects or intramolecular steric hindrance can be reduced by such distortion of the copper(II) coordination polyhedron and/or by changing the geometry of the chelate rings [36].

The calculated mean and standard-deviation values of the in-plane bond lengths around copper(II) are in the same order in all coordination modes. The bond length between copper(II) and the oxygen atom is always shorter than the one between copper(II) and nitrogen in the case when both bind to copper(II), which is due to the smaller atomic radius of oxygen.

Table 14: Means and standard deviations (in parentheses) of Cu–donor in–plane bond lengths [Å] and six valence angles [°] around the copper(II) atom in the coordination polyhedron for the B3LYP optimized geometries.

	cis				trans				2	
	GGp	GpGp	HGp	IGp	GGp	GpGp	HGp	IGp	IGp	IpGp
$Cu-N_{am}$ [Å]	2.06 (±0.01)	2.07 (±0.01)	2.02 (±0.02)		2.03 (±0.01)	2.04 (±0.01)	2.02 (±0.01)			
$Cu-N_{\pi}$ [Å]			2.02 (±0.02)	2.09 (±0.04)			2.04 (±0.01)	2.04 (±0.01)		
$Cu-O^1$ [Å]	1.94 (±0.01)	1.94 (±0.01)		1.94 (±0.02)	1.93 (±0.01)	1.93 (±0.01)		1.95 (±0.02)	2.03 (±0.01)	2.02 (±0.01)
$Cu-O^2$ [Å]									2.10 (±0.04)	2.07 (±0.03)
$Cu-N_{am}'$ [Å]	2.08 (±0.01)	2.07 (±0.01)	2.06 (±0.02)	2.07 (±0.01)	2.04 (±0.01)	2.04 (±0.00)	2.11 (±0.01)	2.03 (±0.02)	2.04 (±0.01)	2.02 (±0.01)
$Cu-O^{1'}$ [Å]	1.94 (±0.01)	1.93 (±0.01)	1.95 (±0.01)	1.95 (±0.01)	1.93 (±0.01)	1.92 (±0.00)	1.95 (±0.01)	1.95 (±0.01)	1.92 (±0.01)	1.90 (±0.01)
$N_{am}-Cu-O^1$ [°]	82.7 (±1.0)	82.4 (±0.7)			84.5 (±0.6)	84.1 (±0.8)				
$N_{am}'-Cu-O^{1'}$ [°]	82.3 (±0.7)	82.7 (±0.7)	82.5 (±0.8)	82.2 (±0.9)	83.9 (±0.6)	84.3 (±0.4)	82.1 (±1.0)	83.09 (±1.08)	84.7 (±0.1)	85.0 (±0.6)
$N_{am}-Cu-N_{am}'$ [°]	99.3 (±1.3)	100.5 (±1.6)	96.6 (±1.1)		176.4 (±3.8)	176.5 (±3.1)	160.7 (±5.0)			
$O^1-Cu-O^{1'}$ [°]	96.2 (±1.3)	95.6 (±0.7)		95.7 (±2.6)	175.8 (±4.3)	177.0 (±3.3)		167.71 (±5.71)	172.0 (±2.4)	169.5 (±10.4)
$N_{am}-Cu-O^{1'}$ [°]	174.8 (±3.6)	172.8 (±5.5)	173.8 (±4.5)		96.9 (±1.2)	95.5 (±0.7)	89.6 (±1.7)			
O^1-Cu-N_{am}' [°]	173.0 (±5.0)	172.7 (±4.9)		163.7 (±8.1)	94.7 (±0.9)	96.3 (±1.5)		91.9 (±3.1)	101.2 (±2.0)	105.0 (±9.2)
$N_{\pi}-Cu-N_{am}$ [°]			91.2 (±1.5)				93.7 (±0.8)			
$N_{\pi}-Cu-O^1$ [°]				89.7 (±2.2)				93.46 (±3.93)		
$N_{\pi}-Cu-O^{1'}$ [°]			91.3 (±1.60)	166.5 (±9.4)			163.0 (±6.7)	92.18 (±1.89)		
$N_{\pi}-Cu-N_{am}'$ [°]			168.7 (±5.75)	96.5 (±2.4)			99.9 (±1.7)	168.43 (±3.74)		
O^1-Cu-O^2 [°]									64.5 (±0.6)	64.8 (±0.3)
$O^2-Cu-O^{1'}$ [°]									109.4 (±1.9)	109.2 (±10.0)
O^2-Cu-N_{am}' [°]									162.9 (± 5.6)	157.5 (±12.4)

3.2.6. COMPARISON WITH PREVIOUS WORK ON Cu(L-HIS)$_2$

In terms of conformer stability behavior, there are no big differences between the Cu(L-His)$_2$ conformers already analyzed [12] (with protonated N_τ) and the structures with protonated N_π treated in this work. In both cases, the *trans* configuration is more stable than the *cis* one for all the coordination modes, except the HG mode. The previous lowest overall energy was determined for a tGG conformer (–1292.76760 a.u.), whereas in this work it is a conformer with the L-His residues in different coordination modes, namely G and Gp. The B3LYP electronic energy of this most stable conformer (tGGp_a19_e12) is –1292.77081 a.u., which is 8.43 kJ mol^{-1} more stable than tGG1. Figure 20 depicts this "old" and "new" global minimum and shows their differences in structure: the (new) tGGp conformer is stabilized by an apical bond formed between Cu and N_π, and a hydrogen bond N_π'–$H_p'\cdots O^{2'}$ in the other L-His residue. These are obviously stronger than the two hydrogen bonds N_{am}–$H_{am}\cdots N_\pi$ present in both L-His side chains in the (old) tGG1 conformer.

<div align="center">

tGG1_te1_te1   tGGp_a19_e12

–1292.76760 a.u.   –1292.77081 a.u.
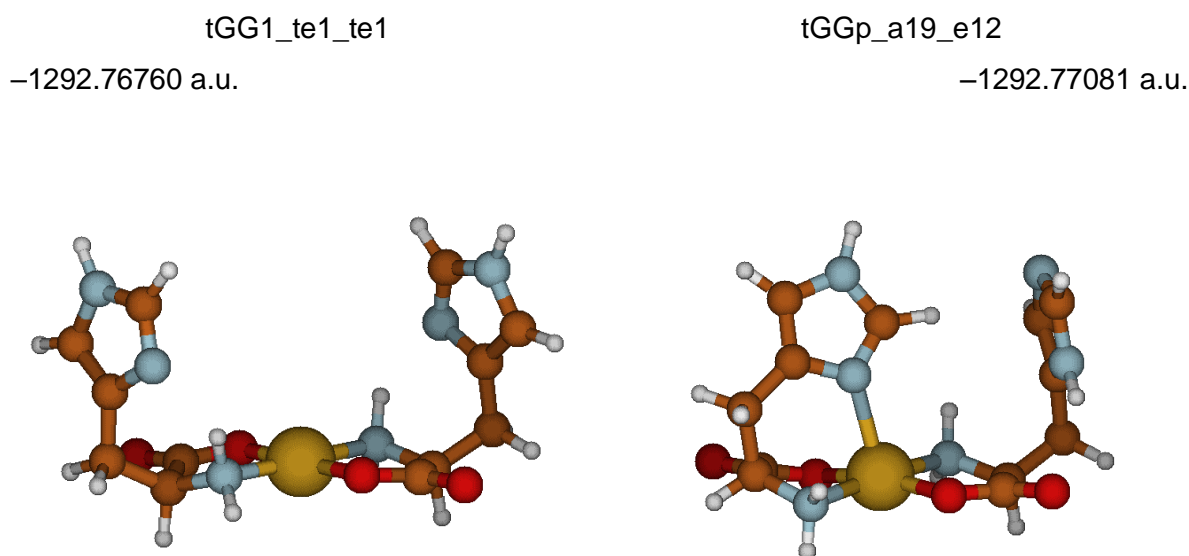
</div>

Figure 20: Comparison of the previously known (left) and the newly found global minimum structure.

The sequence of the energy values of the most stable conformations of each coordination mode was in previous work as follows: tGG1 < tIG1 < cGG1 < cHG1 < cIG1 < tHG1. When the proton is shifted to the other N atom in the imidazole ring, the sequence looks a bit different: tGGp < tGpGp < tIGp < cHGp < cGGp < cGpGp < cIGp < 2IGp < 2IpGp < tHGp. The *2* configuration was not treated in previous work at all, as well as structures with less than four coordinating atoms. The difference between the most stable tGGp and tGpGp conformer is

11.80 kJ mol^{-1}, which means that the previously found global minimum is located between the new ones of lowest and second lowest energy (tGGp$_{min}$ < tGG$_{min}$ < tGpGp$_{min}$).

To separate the energetic effects of the proton shift from N$_\tau$ to N$_\pi$ from those due to the formation of an apical or a hydrogen bond, conformers with very similar geometries but no additional interactions were compared: tGG10 [12], tGGp_a28_a27 (Table 4) and tGpGp_a27_a27 (Table 5). Their energies, -1292.756036 a.u., -1292.753200 a.u. and -1292.750195 a.u., respectively, indicate an accumulative increase in energy of approximately 8 kJ mol^{-1} per proton shift from N$_\tau$ to N$_\pi$. Hence, the formation of an apical bond and a hydrogen bond has a higher effect on the stability than the proton shift.

Concerning the position of the C$^\beta$ atom in the G mode, the axial position in the GG mode is mostly favored in the *cis* conformation, whereas both, the axial and equatorial position are equally abundant in the *trans* conformation. After the proton shift, the equatorial position is preferred in *cis* as well as in the *trans* conformers, which is one of the biggest differences.

When comparing the coordination geometry of the conformers and the apical bonds formed, several similarities can be found. In both analyses, the coordination geometry around copper(II) of the *trans* and *cis* GG (GGp as well as GpGp) conformers is a distorted-planar or in-plane one whereas a distorted tetrahedral coordination is found in the H mode. Also the apical bonds are the same in both: Cu–N$_\pi$ and Cu–N$_{am}$. The comparison of the total amount of stable conformers is not meaningful, because in this work we discussed more conformation possibilities with a larger variation of the angles, which also resulted in much more initial and equilibrium structures.

CONCLUSION

The quantum chemical study of $Cu(L\text{-}His)_2$ as an isolated complex yielded a new most stable conformer (tGGp_a19_e12, Table 4 and Figure 5) with both L-His side chains in the glycine-like mode in *trans* configuration to each other. The conformer with the highest relative B3LYP electronic energy is cGpGp_e33_e33, in which the proton is shifted to N_π in both L-His residues. This conformer in *cis* configuration is 152.5 kJ mol^{-1} less stable than the most stable conformer. It is interesting, that the second most stable conformer from a coordination mode other than GGp is tGpGp_e12_e12_A, which forms the same GpGp coordination mode as the most unstable one. Therefore, the stability depends not only on the position of the proton in the imidazole ring and the coordination mode, but also on the position of the imidazole ring and therefore whether apical bonds or hydrogen bonds are formed. This is in agreement with the analysis of conformers with a very similar geometry but no additional interactions (tGG1 [12], tGGp_a28_a27 (Table 4) and tGpGp_a27_a27 (Table 5)), which shows an energy increase by each proton shift from N_τ to N_π.

By comparing the total number of isolated complex structures in each coordination mode, the highest number of stable conformers is found within the GGp and GpGp mode, due to the freedom of the imidazole ring rotation. The fewest structures remained stable in the HGp and IpGp coordination mode with only 32 and 33 stable conformers with relative energies above 35 and 50 kJ mol^{-1}, respectively.

The eight-membered chelate ring in the Ip mode remained not stable at all, resulting in 33 structures forming a four-membered chelate ring with the two carboxyl oxygen atoms O^1 and O^2 binding to copper(II). The instability of the six-membered chelate ring in the HGp conformers seems to be due to the inflexibility of two atoms, N_τ and C^γ, within the six-membered ring, which are a part of the stiff imidazole ring at the same time. Therefore, the most stable *chair* conformation could not be adopted and many conformations ended up in five- and seven-membered rings (GGp and IGp conformers). The high B3LYP relative electronic energy of these few conformers in the IpGp and HGp coordination mode is related to the high distortion of the planar coordination around copper(II) in direction towards a tetrahedral and trigonal pyramidal geometry. Further, neither interactions with the conjugated imidazole ring system, nor axially binding atoms were detected in these energetically high conformers like it is the case in a number of planar coordination modes. Concerning the hydrogen bonds, most of them were formed in the GGp and GpGp mode, affecting the stability of the isolated complex $Cu(L\text{-}His)_2$ in general.

BIBLIOGRAPHY

1. **J. H. Menkes, M. Alter, G. K. Steigleder, D. R. Weakley, J. Ho Sung.** "A sex-linked recessive disorder with retardation of growth, peculiar hair, and focal cerebral and cerebellar degeneration". *Pediatrics 29 (764–779).* 1962.

2. **D. M. Danks, P. E. Campbell, J. Walker-Smith, B. J. Stevens, J. M. Gillespie, J. Blomfield , B. Turner.** "Menkes' kinky-hair syndrome". *Lancet (1100–1102).* 1972.

3. **D. M. Danks, P. E. Campbell, B. J. Stevens, V. Mayne, E. Cartwright.** "Menkes' kinky hair syndrome. An inherited defect in copper absorption with widespread effects". *Pediatrics 50 (188–201).* 1972.

4. **D. M. Danks, E. Cartwright, B. J. Stevens, R. R. W. Townley.** "Menkes' kinky hair disease: further definition of the defect in copper transport". *Science 179 (1140–1142).* 1973.

5. **A. S. Dekaban, J. K. Steusing.** "Letter: Menkes' kinky hair disease treated with subcutaneous copper sulphate". *Lancet (1523).* 1974.

6. **G. Sherwood, B. Sarkar, A. Sass Kortsak.** "Copper Histidinate Therapy in Menkes Disease: Prevention of Progressive Neurodegeneration". *J. Inher. Meta. Dis. 12 Suppl. 2 (393–396).* 1989.

7. **Z. Tümer, N. Horn, T. Tønnesen, J. Christodoulou, J. T. R. Clarke, B. Sarkar.** "Early copper-histidine treatment for Menkes disease". *Nat. Genet. 12 (11–13).* 1996.

8. **J. Chelly, Z. Turmer, T. Tonnerson, A. Petterson, Y. Ishikawa-Brush, N. Tommerup, N. Horn, A. P. Monaco.** "Isolation of a candidate gene for Menkes disease that encodes a potential heavy metal binding protein". *Nat. Genet. 3 (14–19).* 1993.

9. **J. F. B. Mercer, J. Livingston, B. K. Hall, J. A. Paynter, C. Begy, S. Chandrasekharappa, P. Lockhart, A. Grimes, M. Bhave, D. Siemenack, T. W. Glover.** "Isolation of a partial candidate gene for Menkes disease by positional cloning". *Nat. Genet. 3 (20–25).* 1993.

10. **C. Vulpe, B. Levinson, S. Whitney, S. Packman, J. Gitschier.** "Isolation of a candidate gene for Menkes disease and evidence that it encodes a copper-transporting ATPase". *Nat. Genet. 3 (7–13).* 1993.

11. **M. Marković.** "Molekulsko modeliranje kompleksa bakra(II) s aminokiselinama u vakuumu, kristalu i vodenoj otopini". *Ph.D. thesis, University of Zagreb.* 2012.

12. **M. Marković, M. Ramek, J. Sabolović.** "Why Does the Coordination Mode of Physiological Bis(L-histidinato)copper(II) Differ in the Gas Phase, Crystal Lattice, and Aqueous Solutions? A Quantum Chemical Study". *Eur. J. Inorg. Chem. (198–212).* 2014.

13. **J. Sabolović, M. Ramek, M. Marković.** "Calculating the Geometry and Raman Spectrum of Physiological Bis(L-histidinato)Copper(II): An Assessment of DFT Functionals for Aqueous and Isolated Systems". *J. Mol. Model. 23 (290).* 2017.

14. **M. Ramek, M. Marković, C. Loher, J. Sabolović.** "Pronounced conformational flexibility of physiological (L-histidinato)(L-threoninato)copper(II) in aqueous solution disclosed by a quantum chemical study". *Polyhedron 135 (121–133).* 2017.

15. **M. Marković, M. Ramek, C. Loher, J. Sabolović.** "The Important Role of the Hydroxyl Group on the Conformational Adaptability in Bis(L-threoninato)copper(II) Compared to Bis(L-allo-L-threoninato)copper(II): Quantum Chemical Study". *Inorg. Chem. 55 (7694–7708).* 2016.

16. **M. Marković, C. Loher, M. Ramek, J. Sabolović, I. Mutapčić.** "Computational Study of L-cysteinato-L-asparaginato-copper(II) in Gas Phase". *poster at the 13th Internat. Symposium on Neurology and Neurobiology of Aging in Bregenz.* 2016.

17. **M. Marković, M. Ramek, I. Mutapčić, J. Sabolović.** "Conformational analyses of bis(L-asparaginato)copper(II) in the gas phase and in aqueous solution". *poster at the 11th Triennial Congress of the World Association of Theoretical and Computational Chemistry (WATOC) in Munich.* 2017.

18. **J. Budimčić, M. Ramek, M. Marković, I. Mutapčić, J. Sabolović.** "Quantum chemical study of (L-histidinato)(L-asparaginato)copper(II) in the gas phase and aqueous solution". *poster at the 17th Austrian Chemistry Days in Salzburg.* 2017.

19. **J. T. Rubino, K. J. Franz.** "Coordination chemistry of copper proteins: How nature handles a toxic cargo for essential function". *Journal of Inorganic Biochemistry 107 (129–143).* 2012.

20. **P. Deschamps, P.P. Kulkarni, M. Gautam-Basak, B. Sarkar.** "The saga of copper(II)-L-histidine". *Coordination Chemistry Reviews 249 (895–909).* 2005.

21. **O. Yamauchi, T. Sakurai, A. Nakahara.** "Histidine-Containing Ternary Amino Acid-Copper(II) Complexes. Syntheses and Properties". *Journal of the American Chemical Society, 101, 15 (4164–4172).* 1979.

22. **A. D. Becke.** "Density-functional thermochemistry. III. The role of exact exchange". *J. Chem. Phys. 98 (5648).* 1993.

23. **C. Lee, W. Yang, R.G. Parr.** "Development of the Colle-Salvetti correlation-energy formula into a functional of the electron density". *Phys. Rev. B 37 (785).* 1988.

24. **S. H. Vosko, L. Wilk, M. Nusair.** "Accurate spin-dependent electron liquid correlation energies for local spin density calculations: a critical analysis". *Canadian Journal of Physics 58(8) (1200–1211).* 1980.

25. **P. J. Stephens, F. J. Devlin, C. F. Chabalowski, M. J. Frisch.** "Ab Initio Calculation of Vibrational Absorption and Circular Dichroism Spectra Using Density Functional Force Fields". *J. Phys. Chem., 98 (11623–11627).* 1994.

26. **T. H. Dunning, P. J. Hay.** "Gaussian Basis Sets for Molecular Calculations" in "Methods of Electronic Structure Theory. Vol.3" (H. F. Schaefer III, ed.). *Plenum Press, New York.* 1977.

27. **M. J. Frisch, J. A. Pople.** "Self-consistent molecular orbital methods 25. Supplementary functions for Gaussian basis sets". *J. Chem. Phys. 80 (3265).* 1984.

28. **T. Clark, J. Chandrasekhar, G. W. Spitznagel, P. v. R. Schleyer.** "Efficient Diffuse Function- Augmented Basis Sets for Anion Calculations. III.* The 3-21+G Basis Set for First-Row Elements, Li-F". 1983.

29. **W. R. Wadt, P. J. Hay, R. Willard.** "Ab initio effective core potentials for molecular calculations. Potentials for the transition metal atoms Sc to Hg". *J. Chem. Phys. 82 (270).* 1985.

30. **P. J. Hay, W. R. Wadt.** "Ab initio effective core potentials for molecular calculations. Potentials for main group elements Na to Bi". *J. Chem. Phys. 82 (284).* 1985.

31. **W. R. Wadt, P. J. Hay, R. Willard.** "Ab initio effective core potentials for molecular calculations. Potentials for K to Au including the outermost core orbitals". *J. Chem. Phys. 82 (299).* 1985.

32. **M. J. Frisch et al.** "Gaussian 09 Revision D. 01". *Gaussian Inc. Wallingford CT.* 2009.

33. **J.Gažo, I. B. Bersuker, J. Garaj, M. Kabešová, J. Kohout, H. Langfelderová, M. Melník, M. Serátor, F. Valach.** "Plasticity of the coordination sphere of copper(II) complexes, its manifestation and causes". *Coord. Chem. Rev. 19 (253–297).* 1976.

34. **B. Murphy, B. Hathaway.** "The stereochemistry of the copper(II) ion in the solid-state - some recent perspectives linking the Jahn-Teller effect, vibronic coupling, structure correlation analysis, structural pathways and comparative X-ray crystallography". *Coord. Chem. Rev. 243 (237–262).* 2003.

35. **M. A. Halcrow.** "Jahn-Teller distortions in transition metal compounds, and their importance in functional molecular and inorganic materials". *Chem. Soc. Rev. 42 (1784–1795).* 2013.

36. **J. Sabolović, K. R. Liedl.** "Why Are Copper(II) Amino Acid Complexes Not Planar in Their Crystal Structures? An ab Initio and Molecular Mechanics Study". *Inorg. Chem. 38 (2764–2774).* 1999.